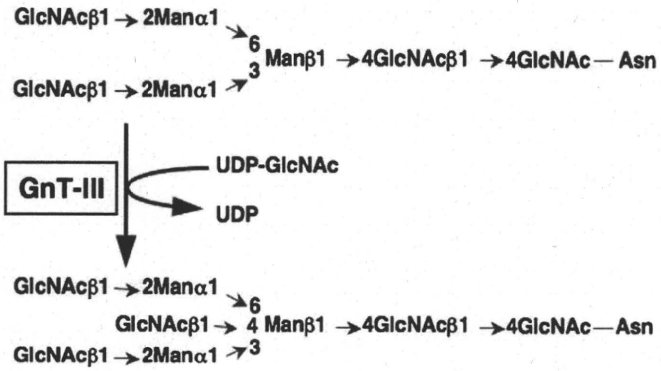

Fig. 1. Bisecting GlcNAc residues in *N*-glycans are synthesized by GnT-III.

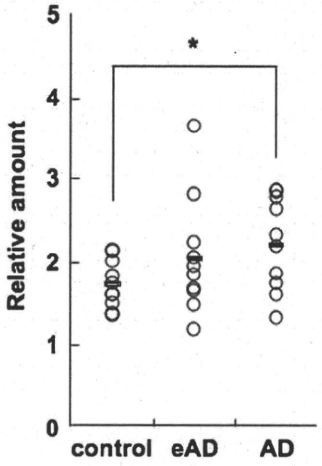

Fig. 2. Quantitative real-time RT-PCR analysis of *GnT-III* mRNA expression in brains of AD patients. Relative amounts of *GnT-III* mRNA were determined in 10 eAD patients, 10 AD patients, and 10 control subjects. All reactions were performed in triplicate and the open circles indicate average values for each individual brain sample. Each horizontal bar indicates the average value of the 10 subjects in that category. Statistically significant differences were identified using the Student's *t*-test ($P = 0.025$) and indicated with an asterisk.

are synthesized. Given the important biological functions of GnT-III (Gu and Taniguchi 2004), we examined the effects of the bisecting GlcNAc on Aβ production and on the activity of the various secretases responsible for Aβ production.

Results

GnT-III mRNA expression in the brains of AD patients

GnT-III catalyzes the transfer of GlcNAc to a core β-mannose residue, producing a bisecting GlcNAc (Wilson et al. 1976; Narasimhan 1982; Nishikawa et al. 1992). To investigate whether GnT-III levels are altered in AD, we measured the amount of *GnT-III* mRNA in the brains of AD patients by quantitative real-time RT-PCR. Preparation of total RNA from non-AD (control), early-stage AD (eAD), or AD brains and real-time RT-PCR analysis was performed as described in *Material and Methods*. As shown in Figure 2, the expression level of *GnT-III* mRNA was significantly increased in AD brains as compared to controls (mean relative amount of control, 1.74; standard deviation (SD), ± 0.28; mean relative amount of AD, 2.23; SD, ± 0.54; $P = 0.025$, Student's *t*-test). However, there was no statistically significant difference in *GnT-III* mRNA levels when comparing eAD brains to controls (mean relative amount of eAD, 2.06; SD, ± 0.68, $P = 0.21$, Student's *t*-test), or when comparing eAD brains to AD brains ($P = 0.56$, Student's *t*-test). Taken together, these results suggest that *GnT-III* mRNA expression increases with disease progression. Therefore, it is conceivable that the number of *N*-glycans having a bisecting GlcNAc residue is increased in AD brains.

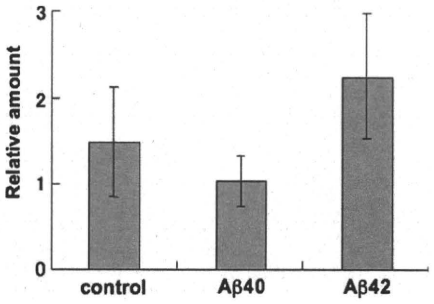

Fig. 3. Relative levels of *GnT-III* mRNA expression after incubation with Aβ. All reactions were performed in quadruplicate. Aβ40 or Aβ42 was added to Neuro2a cell culture medium at a final concentration of 2 μg/mL. After 48 h incubation, cells were harvested for RNA preparation followed by quantitative real-time RT-PCR. Average values ± 1 SD are shown.

Aβ42 exposure enhances GnT-III expression

We examined whether incubation with Aβ40 or Aβ42 affected *GnT-III* mRNA expression levels. Thus, after Aβ40 or Aβ42 was added to the culture media of Neuro2a cells, *GnT-III* expression level was analyzed by quantitative real-time RT-PCR (Figure 3). Compared to control cells (mean relative amount, 1.48; SD, ± 0.64), Aβ42 enhanced the *GnT-III* mRNA expression approximately 1.5-fold (mean relative amount, 2.24; SD, ± 0.72); in contrast, Aβ40 decreased the *GnT-III* expression (mean relative amount, 1.02; SD, ± 0.3). These results indicate that Aβ42, but not Aβ40, enhances GnT-III mRNA expression.

Effect of GnT-III on APP processing

According to our prior (Akasaka-Manya et al. 2008) and current (Figure 2) studies, it is likely that increased *GnT-III* mRNA levels increase the number of *N*-glycans having a bisecting GlcNAc residue. Therefore, we prepared stable transfectants of Neuro2a mouse neuroblastoma cells that express GnT-III by using an expression plasmid encoding *GnT-III*. The microsomal membrane fraction from the transfected cells was used as an enzyme source to measure GnT-III activity (Figure 4A). GnT-III activity was significantly increased in cells transfected with *GnT-III* (32.1 pmol/min/mg) as compared to cells transfected with the "empty" pCXN2 vector (mock transfectant, 0.1 pmol/min/mg). As expected, the intensity of staining by the *Phaseolus vulgaris* lectin E_4 ($PHA\text{-}E_4$), which specifically recognizes bisecting GlcNAc residues (Yamashita et al. 1983), was enhanced in cellular proteins prepared from *GnT-III*-transfected cells (Figure 4B), demonstrating that these proteins have a higher content of bisecting GlcNAc residues. There were no significant differences in the expression levels of membrane-bound APP and secreted APP (sAPP) (Figure 4C, upper-left panel and upper-right

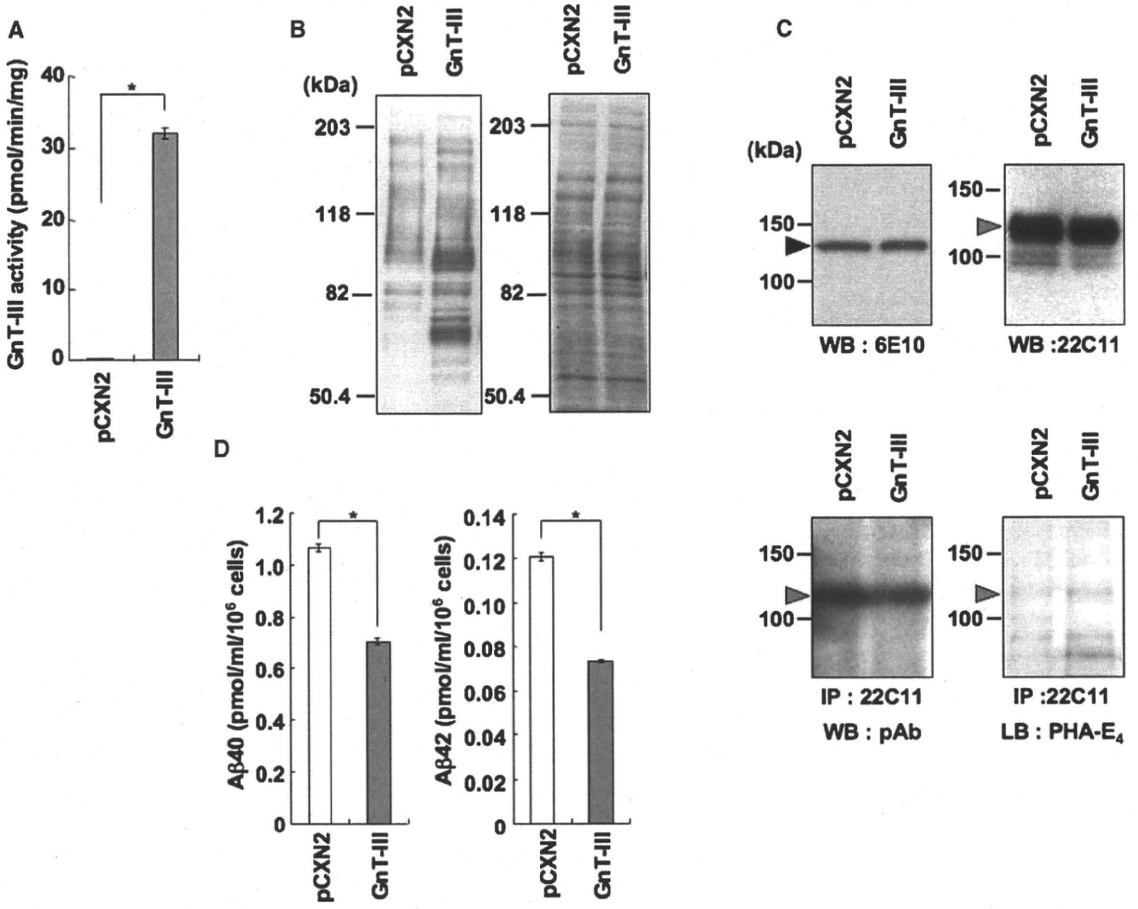

Fig. 4. Overexpression of *GnT-III* mRNA induces an increase in bisecting GlcNAc residues on cellular proteins and a decrease in Aβ secretion. (**A**) GnT-III activities of Neuro2a cells transfected with a *GnT-III* expression vector or an empty vector (pCXN2). Average values ± 1 SD of three independent experiments are shown. Asterisks indicate statistically significant differences ($P < 0.01$, Student's *t*-test). (**B**) Lectin (PHA-E_4) blot analysis of microsomal fraction of Neuro2a cells transfected with a *GnT-III* expression vector or an empty vector (pCXN2). Elevation of the bisecting GlcNAc modification was observed in *GnT-III*-transfected cells. Right panel indicates protein-staining patterns by Coomasie brilliant blue (CBB). Molecular weight standards are shown on the left. (**C**) Western blot analysis of membrane-bound APP or secreted APP (sAPP) in culture supernatants of Neuro2a cells transfected with a *GnT-III* expression vector or an empty vector (pCXN2). Membrane-bound APP was detected with an anti-APP monoclonal antibody (6E10) (upper-left panel) and sAPP in culture supernatant with an anti-APP monoclonal antibody (22C11) (upper-right panel). sAPP was immunoprecipitated from culture supernatant with an anti-APP monoclonal antibody (22C11), and then detected on blots by either an anti-APP polyclonal antibody (pAb, lower-left panel) or by the PHA-E_4 lectin (lower-right panel). Black triangle indicates membrane-bound APP and gray triangles indicate sAPP. Molecular weight standards are shown on the left. (**D**) The effect of GnT-III overexpression on Aβ production by transfected Neuro2a cells. Concentrations of Aβ40 (left) and Aβ42 (right) in culture supernatants were determined by ELISA. The average values ± 1 SD of three independent experiments are shown. Asterisks indicate statistically significant differences ($P < 0.01$, Student's *t*-test). pCXN2: stable mock transfectant of Neuro2a cells; GnT-III: stable transfectant of Neuro2a cells expressing GnT-III.

panel, respectively), but the intensity of PHA-E_4 staining of sAPP was enhanced in cells transfected with *GnT-III* (Figure 4C, lower-right panel). These results demonstrate that APP secreted from *GnT-III*-transfected cells has a higher content of bisecting GlcNAc residues.

We then measured levels of Aβ secreted by Neuro2a cells expressing recombinant GnT-III (Figure 4D). The concentrations of Aβ40 and Aβ42 secreted from the mock transfectant were 1.08 pmol/mL/10^6cells and 0.12 pmol/mL/10^6cells, respectively. For the *GnT-III* transfectant, the concentrations of Aβ40 and Aβ42 were 0.69 pmol/mL/10^6cells and 0.07 pmol/mL/10^6cells, respectively; these were 36.2% and 42.7% lower than those from the mock transfectant. These statistically significant results indicate that increased cellular expression of GnT-III significantly downregulates the secretion of Aβ peptides.

Western blot analysis of secretases

Contrary to our expectations, increased modification of *N*-glycans by bisecting GlcNAc downregulated Aβ secretion (Figure 4D). At least two mechanisms by which increased bisecting GlcNAc could reduce Aβ production should be considered. One possibility is that increasing bisecting GlcNAc expression on APP affects the conformation of APP, changing its susceptibility to α-, β-, and/or γ-secretase, and/or the intracellular localization of APP. Another possibility is that increasing the bisecting GlcNAc content of the secretases affects their enzymatic activity. α-Secretase activity is encoded by two proteins: ADAM 10 (a disintegrin and metalloproteinase 10) and tumor necrosis factor-α converting enzyme (TACE or, equivalently, ADAM 17). TACE has six potential *N*-glycosylation sites (Moss et al. 1997). ADAM 10 has four potential *N*-glycosylation sites, and their *N*-glycans are crucial for processing, localization, and

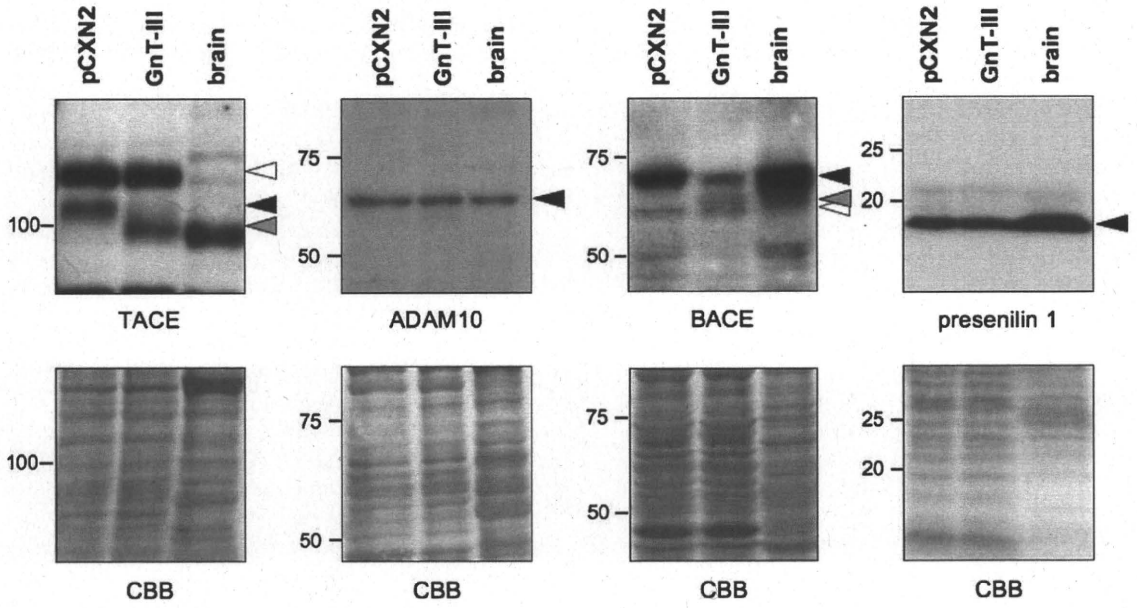

Fig. 5. Western blot analysis of various secretases (TACE, ADAM10, BACE, and presenilin) in *GnT-III*-transfected Neuro2a cells. For TACE and BACE, black and gray triangles indicate mature forms and white triangles indicate immature forms. For ADAM10 and presenilin 1, black triangles indicate the migration positions of ADAM10 and the C-terminal fragment of presenilin 1, respectively. Molecular weight standards are shown on the left. pCXN2: stable mock transfectant of Neuro2a cells; GnT-III: stable transfectant of Neuro2a cells expressing recombinant GnT-III; brain: mouse brain membrane fraction. Bottom figures indicate protein-staining patterns by CBB corresponding to each upper panel.

activity (Escrevente et al. 2008). BACE (β-site APP cleaving enzyme), which possesses β-secretase activity, has four potential *N*-glycosylation sites, three of them appear to be glycosylated (Charlwood et al. 2001). γ-Secretase is a protein complex consisting of presenilin, nicastrin, APH-1, and PEN-2. Nicastrin has 16 potential *N*-glycosylation sites, although inhibition of complex *N*-glycan processing does not affect γ-secretase activity (Herreman et al. 2003).

To clarify the mechanism(s) responsible for downregulating Aβ secretion, the expression levels of the secretases were measured. TACE is reported to change from an immature to a mature form (Milla et al. 1999; Schlondorff et al. 2000; Peiretti et al. 2003). Our Western blot analysis of TACE expressed by Neuro2a cells showed two major bands (Figure 5, left lane); results with proteins isolated from normal mouse brain are shown for comparison. The upper band (white triangle) corresponds to immature TACE bearing high-mannose *N*-glycans; the lower band corresponds to mature TACE (black triangle). Although two TACE bands were also observed in *GnT-III*-transfected Neuro2a cells (Figure 5, right lane), the mobility of mature TACE (gray triangle) from *GnT-III*-transfected cells was faster than that from the mock transfectant. As reported previously, this type of finding is a unique feature seen by introducing bisecting GlcNAc into glycoprotein *N*-glycans (Shigeta et al. 2006). In addition, the expression level of TACE in *GnT-III*-transfected cells was nearly the same as compared with mock transfectant. BACE is also reported to change from an immature form to a mature form (Benjannet et al. 2001; Schmechel et al. 2004). Our Western blot analysis of Neuro2a cells showed two BACE bands (Figure 5, left lane). The upper band corresponds to mature BACE (black triangle) and the lower to immature BACE (white triangle). An additional new band of intermediate mobility appeared in the *GnT-III*-transfected cells (Figure 5, gray triangle in the right lane). Interestingly, in the *GnT-III* transfectant, the molecular size and expression of BACE both decreased. In contrast, when comparing the mock transfectant with the *GnT-III* transfectant, no differences in the expression level or molecular size of ADAM 10 or the C-terminal fragment of presenilin 1 were seen (Thinakaran et al. 1996) (Figure 5). Taken together, these results suggest that changing the *N*-glycans of TACE and BACE may affect α- and β-secretase activities.

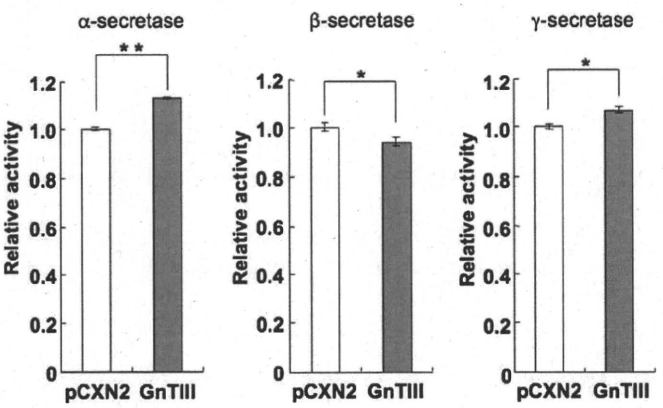

Fig. 6. Secretase activities in *GnT-III*-transfected Neuro2a cells. α-, β-, and γ-secretase activities (left, middle and right panels, respectively) were determined. For comparison, the fluorescence intensity of the pCXN2 transfectant was set to 1.0. The average percentages ± 1 SD of three independent experiments are shown. Asterisks indicate statistically significant differences ($^{*}P < 0.01$, $^{**}P = 0.0001$, Student's *t*-test).

Secretase assays

To examine the effect of *N*-glycan changes of TACE and BACE on enzymatic activity, we measured α- and β-secretase activities in *GnT-III* transfectants of Neuro2a cells. As shown in Figure 6, in the *GnT-III* transfectant, α-secretase activity (113% of the

activity of the control pCXN2 transfectant, $P = 0.0001$) was slightly upregulated, but β-secretase activity (97% of the pCXN2 transfectant, $P = 0.042$) was modestly downregulated. Because changes in γ-secretase activity may also affect Aβ production, its activity in *GnT-III*-transfected cells was measured; modest upregulation was observed (107% of the pCXN2 transfectant, $P = 0.015$). Taken together, the increased α-secretase activity and decreased β-secretase activity in the *GnT-III* transfectant were the most probable cause of the reduction in Aβ production shown in Figure 4D. Thus, these results suggest that changes in *N*-glycan of TACE and BACE affect their enzymatic activities and lead to downregulation of Aβ production.

Discussion

In previous studies, we described the *N*-glycan structures of APP695 produced by Chinese hamster ovary cells (Sato et al. 1999) and the C17.2 mouse neural stem cell line (Akasaka-Manya et al. 2008). Recombinant APP695 in both cell lines had sialylated bi- and triantennary complex-type *N*-glycans with fucosylated and nonfucosylated trimannosyl cores. However, only APP695 produced by C17.2 cells had *N*-glycans containing bisecting GlcNAc. This may be due to cell-type-specific differences in *N*-glycan processing that can be found with various recombinant glycoproteins (Kagawa et al. 1988; Cumming 1991). To determine whether mutations in the *APP* gene alter the structures of processed *N*-glycans, we expressed two mutant recombinant APPs (i.e., the Swedish type and the London type) in transfected C17.2 cells. Structural analysis of these *N*-glycans revealed that the two mutant APPs had higher contents of bisecting GlcNAc and core-fucose residues as compared to wild-type APP. These results clearly showed that these slight changes in amino acid sequence affected *N*-glycan processing.

The glycosyltransferase responsible for adding the bisecting GlcNAc residue is GnT-III (Wilson et al. 1976; Narasimhan 1982; Nishikawa et al. 1992). To examine whether *GnT-III* mRNA levels are related to the pathogenesis of sporadic AD, we examined this issue by quantitative real-time RT-PCR using brains of normal individuals and AD patients. As shown in Figure 2, *GnT-III* mRNA levels were significantly increased in the brains of AD patients. This upregulation may affect AD pathogenesis because significant differences were found in patients with an advanced stage of AD. Interestingly, incubation of Neuro2a cells with Aβ42 increased *GnT-III* gene expression levels (Figure 3). In a recent report (Fiala et al. 2007), exposure of normal peripheral blood mononuclear cells to Aβ peptide upregulated transcription of *GnT-III* and led to increased Aβ clearance by phagocytosis; interestingly, mononuclear cells isolated from AD patients exhibited downregulated *GnT-III* gene expression and were defective in phagocytosis of Aβ. Since upregulation of GnT-III expression was associated with enhanced phagocytosis of Aβ, an increment of GnT-III levels in mononuclear cells may lead to improved Aβ clearance. In contrast, as reported here, increased expression of GnT-III in Neuro2a cells downregulated Aβ production (Figure 4D), and *GnT-III* mRNA levels were increased in AD brains (Figure 2). Taken together, these results suggest that upregulation of GnT-III in neuronal cells may diminish Aβ production in AD brains. In addition, expression of GnT-III in neurons and monocytes may modulate Aβ accumulation by different mechanisms. That is, upregulation of GnT-III expression in monocytes may enhance Aβ clearance, and increased GnT-III expression in neuronal cells may inhibit Aβ production. Taken together, both responses may be adaptive, protective responses that inhibit the further progression of AD.

To evaluate the mechanism by which an increased number of bisecting GlcNAc residues could reduce Aβ production, several possibilities should be considered. As reported here, the APP secreted by *GnT-III*-transfected Neuro2a cells has a higher content of bisecting GlcNAc than that secreted by control cells (Figure 4C). The addition of bisecting GlcNAc may affect the conformation of APP, thereby leading to a change in its susceptibility to α-, β-, and/or γ-secretases. Alteration of glycoprotein glycans is known to affect various properties of a given protein including its susceptibility to various modifying enzymes. For example, organ-specific differential glycosylation of low-density lipoprotein receptor-related protein 1 (LRP1) alters its proteolytic cleavage by γ-secretase (May et al. 2003). In addition, increased sialylation of APP enhanced Aβ secretion (Nakagawa et al. 2006). Bisecting GlcNAc residues are also known to affect the branching and elongation of various *N*-glycans antennae (Narasimhan 1982; Schachter et al. 1983; Schachter 1986). Therefore, it is possible that increasing bisecting GlcNAc expression on APP leads to changes in the APP *N*-glycan structure, including less sialylation, which may alter it susceptibility to cleavage by individual secretases (Fukuta et al. 2000; Koyota et al. 2001). Furthermore, because changing the *N*-glycan structure can alter intracellular glycoprotein localization, it is possible that bisecting GlcNAc affects APP trafficking and, thereby, its susceptibility to secretases. For example, in cells that overexpress GnT-III, cell surface turnover of E-cadherin is delayed (Yoshimura et al. 1996). In contrast, the cell surface expression of epidermal growth factor receptor is reduced in GnT-III overexpressing cells (Rebbaa et al. 1997). In addition, APP localization and trafficking vary according to its glycan modifications (McFarlane et al. 1999).

Another possibility is that increasing the bisecting GlcNAc content of the secretases affects their enzymatic activity. For example, glycosylation is known to play a critical role in maintaining the enzymatic activity of β-secretase (Charlwood et al. 2001). In that study, baculovirus-expressed β-secretase, which only has high-mannose-type *N*-glycans, exhibits only ~50% of the activity found when the enzyme is expressed by mammalian cells, when it has complex-type *N*-glycans (Charlwood et al. 2001). To investigate this issue, we measured secretase activities in *GnT-III*-transfected cells; α- and β-secretase activities were significantly increased and decreased, respectively (Figure 6). By Western blot analysis, the *N*-glycan structures of TACE and BACE are altered (Figure 5), perhaps explaining the changes in their enzymatic activities. In a previous study (Skovronsky et al. 2001), TACE-expressing neurons often colocalized with Aβ plaques. Our results showed that GnT-III expression was increased in AD brains (Figure 2) and that increases in GnT-III might decrease BACE expression (Figure 6). Taken together, it is likely that upregulation of GnT-III in AD brains induces changes in the APP processing enzymes, TACE and BACE, which may inhibit Aβ formation. Although the detailed mechanisms are not yet clear, this increased expression of GnT-III may homeostatically partially protect AD brains from further Aβ production.

Bisected *N*-glycans play important roles in neurological function in vitro and in vivo. For example, bisecting GlcNAc

regulated serum depletion-induced neuritogenesis (Shigeta et al. 2006). In addition, truncated, inactive GnT-III induced abnormal neurological phenotypes in mice (Bhattacharyya et al. 2002). As another example, changes in bisected *N*-glycans may be related to the pathogenesis of prion disease (Rudd et al. 1999). Therefore, further studies are required to understand the precise physiological and pathological roles of bisecting GlcNAc in brain development and function.

In summary, based on the current results, we propose that high expression of GnT-III in human AD brains reduces Aβ production and protects against further deterioration of neurological function during this disease process. Therefore, compounds that upregulate the expression of bisecting *N*-glycans may provide a novel therapeutic approach toward preventing or ameliorating AD.

Material and methods

Patients and controls

Human brain tissues were obtained from the Brain Bank for Aging Research (BBAR), which consists of consecutive autopsy cases from a general geriatric hospital with informed consent obtained from the relatives for each autopsy. The brains were handled using the BBAR protocol described previously (Fumimura et al. 2007). In brief, half of the brain was serially sections into 7 mm slices, snap-frozen using powdered dry ice, and stored at −80°C. To minimize RNA degradation, samples with the shortest postmortem intervals were selected for study. Two grams of frozen gray matter were sampled from the temporal pole of 10 cases each with AD, eAD, and age-matched normal controls. The diagnosis of AD was based on the BBAR criteria (Hughes et al. 1982; Murayama and Saito 2004), as follows: (1) clinical dementia rating (Hughes et al. 1982) $\geq$ 1; (2) Braak's senile plaque stage equal to C; and (3) the Braak's neurofibrillary tangle stage $\geq$ IV. The diagnosis of eAD was based on the following criteria: (1) clinical dementia rating, either 0 or 0.5; (2) Braak's senile plaque stage $\geq$ B; and (3) Braak's neurofibirillary tangle stage $\geq$ III. The criteria for designating brains as coming from normal controls included a clinical dementia rating of 0, Braak's senile plaque stage 0, and Braak's neurofibrillary tangle stage $\leq$ II. The age of the selected AD cases ranged from 79 to 98 years old (average of 88.2 years), and the postmortem interval from 1.8 to 17.7 h (average of 7.1 h). The age of the eAD cases ranged between 76 and 96 years (average of 90.3 years), and the postmortem interval between 1.2 and 39.9 h (average of 9.6 h). The age of the normal controls ranged from 68 to 86 years (average of 75.8 years), and the postmortem interval ranged from 1.5 to 29.1 h (average of 7.4 h). This study was approved by the Internal Review Board of Tokyo Metropolitan Institute of Gerontology and of Tokyo Metropolitan Geriatric Hospital.

Real-time RT-PCR analysis

Total RNA was isolated from a portion of each patient's brain using the guanidinium thiocyanate method with TRIzol (Invitrogen Corp., Carlsbad, CA), following the manufacturer's instructions. The integrity of the isolated total RNA was confirmed using an Agilent 2100 bioanalyzer (Agilent Technologies, Inc., Santa Clara, CA). Total RNA from Neuro2a cells was isolated using ISOGEN (Nippon Gene Co., Ltd, Tokyo, Japan), following the manufacturer's instructions. First-strand cDNAs were synthesized using 5 μg of total RNA, SuperScript II RNase H^- Reverse Transcriptase, and random primers (Invitrogen). The relative quantification of target mRNA was determined using a TaqMan real-time RT-PCR assay on a 7300 Fast Real-Time PCR System (Applied Biosystems, Foster City, CA), following the manufacturer's instructions using the TaqMan Universal PCR Master Mix and TaqMan Gene Expression Assays (i.e., a mixture of designed primers and TaqMan probes, Applied Biosystems): *GnT-III*, Hs02379589_s1; endogenous control, the TaqMan Ribosomal RNA Control Reagents VIC Probe. 18S rRNA was used as normalization control.

Cell culture and expression of GnT-III

Neuro2a mouse neuroblastoma cells were maintained in a mixture of Dulbecco's modified Eagle's medium and OptiMEM (1:1, v/v, Invitrogen) supplemented with 5% fetal bovine serum (Invitrogen), 2 mM L-glutamine, 100 units/mL penicillin, and 50 μg/mL streptomycin at 37°C in a 5% CO_2 atmosphere. The pCXN2-rat-*GnT-III* expression plasmid was described previously (Kitada et al. 2001). This plasmid was transfected into Neuro2a cells using Lipofectamine PLUS reagent (Invitrogen) according to the manufacturer's instructions. Stable transfectants were selected with G418 (Invitrogen) at 1 mg/mL. The culture supernatants of these transfectants were collected after 24 h incubation in Dulbecco's modified Eagle's medium:OptiMEM (1:1, v/v) supplemented with 0.2% fetal bovine serum. The cells were homogenized in 10 mM Tris-HCl, pH 7.4, 1 mM EDTA, 250 mM sucrose, 1 mM dithiothreitol, with protease inhibitor mixture (3 μg/mL pepstatin A, 1 μg/mL leupeptin, 1 mM benzamidine-HCl, 1 mM PMSF). After centrifugation at 900 × *g* for 10 min, the supernatant was centrifuged at 100,000 × *g* for 1 h; the pellet was used as the microsomal fraction. Protein concentration was determined by BCA assay (Thermo Fisher Scientific Inc., Waltham, MA).

Aβ treatment of Neuro2a cells was performed as follows: Aβ40 and Aβ42 were each purchased from PEPTIDE INSTITUTE, INC. (Osaka, Japan) and dissolved in H_2O. Aβ40 or Aβ42 were added to culture medium at a final concentration of 2 μg/mL. Cells were cultured for 48 h and harvested for RNA preparation followed by real-time RT-PCR.

Preparation of mouse brain membrane fraction

Brains were obtained from 4-week-old C57BL/6 mice, and homogenized with 9 volumes (weight/volume) of 10 mM Tris-HCl, pH 7.4, 1 mM EDTA, 250 mM sucrose. After centrifugation at 900 × *g* for 10 min, the supernatant was centrifuged at 100,000 × *g* for 1 h; the pellet was used as the microsomal membrane fraction. Protein concentration was determined by BCA assay. All experimental procedures using laboratory animals were approved by the Animal Care and Use Committee of Tokyo Metropolitan Institute of Gerontology.

Assay for GnT-III activity

GnT-III activity was measured using a modification of a previously reported method (Taniguchi et al. 1989). The enzyme assay mixture, containing 125 mM MES buffer (pH 6.25), 200 mM GlcNAc, 10 mM $MnCl_2$, 20 mM UDP-GlcNAc, 0.5% Triton X-100, 10 μM of 2-aminobenzamide-labeled [GlcNAcβ1-2Manα1-6 (GlcNAcβ1-2Manα1-3) Manβ1-4Glc

NAcβ1-4GlcNAc] (ProZyme, Leandro, CA), and cell homogenate were incubated at 37°C for 1 h. After boiling for 3 min to stop the reaction, the mixture was subjected to reversed-phase HPLC using a Cosmosil 5C18-AR column (Nacalai Tesque, Kyoto, Japan), which was equilibrated with the 100 mM ammonium acetate buffer, pH 4.0, and eluted with a gradient of 1-butanol (0.25–1% butanol) over 120 min at a flow rate of 1 mL/min at 55°C.

Immunoprecipitation

For APP immunoprecipitation, culture supernatants were mixed with an anti-APP monoclonal antibody (22C11, Millipore, Billerica, MA). After incubation at 4°C for 2 h, Protein G-coupled Sepharose-4B beads (GE Healthcare UK Ltd., Buckinghamshire, England) were added and the mixture rotated at 4°C for 2 h. The beads were washed three times with PBS and suspended in the sample buffer. Immunoprecipitated proteins were recovered by boiling for 3 min and then subjected to Western blot and lectin blot analyses.

Western blot analysis

Proteins were separated by SDS–PAGE (for TACE, a 5–10% gradient gel; for APP, BACE, and ADAM 10, a 7.5% gel; for presenilin 1, a 12.5% gel) and transferred to a PVDF membrane. The membrane, after blocking in PBS containing 5% skim milk and 0.05% Tween 20, was incubated with an anti-APP polyclonal antibody (Millipore, Billerica, MA) or an anti-APP monoclonal antibody (6E10, Signet laboratories, Dedham, MA). The membrane was then incubated with anti-rabbit IgG conjugated with horseradish peroxidase (GE Healthcare). Antibody-bound proteins were visualized using an ECL kit (GE Healthcare).

Secretases in the microsomal fractions were visualized after separation by SDS–PAGE using anti-TACE polyclonal antibody (Thermo Fisher Scientific), anti-ADAM10 antibody, anti-presenilin 1 antibody, and anti-BACE antibody (Abcam, Cambridge, England).

Lectin blot analysis

Immunoprecipitated proteins were separated by SDS–PAGE and transferred to a PVDF membrane. After blocking with 3% bovine serum albumin (BSA, Nacalai Tesque) in 10 mM Tris-HCl (pH 7.4) containing 140 mM NaCl, 1 mM $CaCl_2$, 1 mM $MgCl_2$, 1 mM $MnCl_2$, and 0.05% Tween 20 (TBS-T), the membrane was incubated with biotin-conjugated PHA-E_4 (Seikagaku Corporation, Tokyo, Japan) in TBS-T containing 1% BSA. After treating the membrane with the Vectastain ABC kit (Vector, Burlingame, CA), lectin-bound proteins were visualized with an ECL kit.

Quantification of soluble Aβ by sandwich ELISA

Culture supernatants were subjected to enzyme-linked immunosorbent assay (ELISA) using the Human/Rat β-Amyloid 40 ELISA kit II and the Human/Rat β-Amyloid 42 ELISA kit High Sensitive (Wako Pure Chemical Industries, Ltd., Osaka, Japan) according to manufacturer's instructions.

Secretase assays

Secretase enzymatic assays were performed using the α-secretase assay kit, β-secretase assay kit, and γ-secretase assay kit (R & D Systems, Inc., Minneapolis, MN), according to manufacturer's instructions. Briefly, cultured Neuro2a cells were harvested and cell numbers counted. Cells were lysed with the extraction buffer and used as an enzyme source for the assay. An APP peptide conjugated to fluorescent reporter and quencher was used as the substrate. The protein content of cell lysates was determined by BCA assay and secretase activities were normalized to protein concentration.

Funding

The Japan Society for the Promotion of Science (20390031).

Acknowledgements

We thank Ms. Harumi Yamamoto and Ms. Reiko Fujinawa for technical assistance.

Conflict of interest statement

None declared.

Abbreviations

Aβ, β-amyloid; AD, Alzheimer's disease; ADAM, a disintegrin and metalloprotease; APP, amyloid precursor protein; BACE, β-site APP-cleaving enzyme; eAD, early-stage AD; GnT, *N*-acetylglucosaminyltransferase; TACE, tumor necrosis factor-α-converting enzyme.

References

Akasaka-Manya K, Manya H, Sakurai Y, Wojczyk BS, Spitalnik SL, Endo T. 2008. Increased bisecting and core-fucosylated *N*-glycans on mutant human amyloid precursor proteins. *Glycoconj J.* 25:775–786.

Benjannet S, Elagoz A, Wickham L, Mamarbachi M, Munzer JS, Basak A, Lazure C, Cromlish JA, Sisodia S, Checler F, et al. 2001. Post-translational processing of β-secretase (β-amyloid-converting enzyme) and its ectodomain shedding. The pro- and transmembrane/cytosolic domains affect its cellular activity and amyloid-β production. *J Biol Chem.* 276:10879–10887.

Bhattacharyya R, Bhaumik M, Raju TS, Stanley P. 2002. Truncated, inactive *N*-acetylglucosaminyltransferase III (GlcNAc-TIII) induces neurological and other traits absent in mice that lack GlcNAc-TIII. *J Biol Chem.* 277:26300–26309.

Charlwood J, Dingwall C, Matico R, Hussain I, Johanson K, Moore S, Powell DJ, Skehel JM, Ratcliffe S, Clarke B, et al. 2001. Characterization of the glycosylation profiles of Alzheimer's β-secretase protein Asp-2 expressed in a variety of cell lines. *J Biol Chem.* 276:16739–16748.

Citron M, Oltersdorf T, Haass C, McConlogue L, Hung AY, Seubert P, Vigo-Pelfrey C, Lieberburg I, Selkoe DJ. 1992. Mutation of the β-amyloid precursor protein in familial Alzheimer's disease increases β-protein production. *Nature.* 360:672–674.

Cumming DA. 1991. Glycosylation of recombinant protein therapeutics: Control and functional implications. *Glycobiology.* 1:115–130.

Escrevente C, Morais VA, Keller S, Soares CM, Altevogt P, Costa J. 2008. Functional role of *N*-glycosylation from ADAM10 in processing, localization and activity of the enzyme. *Biochim Biophys Acta.* 1780:905–913.

Fiala M, Liu PT, Espinosa-Jeffrey A, Rosenthal MJ, Bernard G, Ringman JM, Sayre J, Zhang L, Zaghi J, Dejbakhsh S, et al. 2007. Innate immunity and transcription of MGAT-III and Toll-like receptors in Alzheimer's disease patients are improved by bisdemethoxycurcumin. *Proc Natl Acad Sci USA.* 104:12849–12854.

Fukuta K, Abe R, Yokomatsu T, Omae F, Asanagi M, Makino T. 2000. Control of bisecting GlcNAc addition to *N*-linked sugar chains. *J Biol Chem.* 275:23456–23461.

Fumimura Y, Ikemura M, Saito Y, Sengoku R, Kanemaru K, Sawabe M, Arai T, Ito G, Iwatsubo T, Fukayama M, et al. 2007. Analysis of the adrenal gland is useful for evaluating pathology of the peripheral autonomic nervous system in Lewy body disease. *J Neuropathol Exp Neurol.* 66:354–362.

Gu J, Taniguchi N. 2004. Regulation of integrin functions by *N*-glycans. *Glycoconj J.* 21:9–15.

Herreman A, Van Gassen G, Bentahir M, Nyabi O, Craessaerts K, Mueller U, Annaert W, De Strooper B. 2003. γ-Secretase activity requires the presenilin-dependent trafficking of nicastrin through the Golgi apparatus but not its complex glycosylation. *J Cell Sci.* 116:1127–1136.

Hughes CP, Berg L, Danziger WL, Coben LA, Martin RL. 1982. A new clinical scale for the staging of dementia. *Br J Psychiatry.* 140:566–572.

Kagawa Y, Takasaki S, Utsumi J, Hosoi K, Shimizu H, Kochibe N, Kobata A. 1988. Comparative study of the asparagine-linked sugar chains of natural human interferon-β 1 and recombinant human interferon-β 1 produced by three different mammalian cells. *J Biol Chem.* 263:17508–17515.

Kitada T, Miyoshi E, Noda K, Higashiyama S, Ihara H, Matsuura N, Hayashi N, Kawata S, Matsuzawa Y, Taniguchi N. 2001. The addition of bisecting *N*-acetylglucosamine residues to E-cadherin down-regulates the tyrosine phosphorylation of β-catenin. *J Biol Chem.* 276:475–480.

Koyota S, Ikeda Y, Miyagawa S, Ihara H, Koma M, Honke K, Shirakura R, Taniguchi N. 2001. Down-regulation of the α-Gal epitope expression in *N*-glycans of swine endothelial cells by transfection with the *N*-acetylglucosaminyltransferase III gene. Modulation of the biosynthesis of terminal structures by a bisecting GlcNAc. *J Biol Chem.* 276:32867–32874.

May P, Bock HH, Nimpf J, Herz J. 2003. Differential glycosylation regulates processing of lipoprotein receptors by γ-secretase. *J Biol Chem.* 278:37386–37392.

McFarlane I, Georgopoulou N, Coughlan CM, Gillian AM, Breen KC. 1999. The role of the protein glycosylation state in the control of cellular transport of the amyloid β precursor protein. *Neuroscience.* 90:15–25.

Milla ME, Leesnitzer MA, Moss ML, Clay WC, Carter HL, Miller AB, Su JL, Lambert MH, Willard DH, Sheeley DM, et al. 1999. Specific sequence elements are required for the expression of functional tumor necrosis factor-α-converting enzyme (TACE). *J Biol Chem.* 274:30563–30570.

Moss ML, Jin SL, Milla ME, Bickett DM, Burkhart W, Carter HL, Chen WJ, Clay WC, Didsbury JR, Hassler D, et al. 1997. Cloning of a disintegrin metalloproteinase that processes precursor tumour-necrosis factor-α. *Nature.* 385: 733–736.

Murayama S, Saito Y. 2004. Neuropathological diagnostic criteria for Alzheimer's disease. *Neuropathology.* 24:254–260.

Nakagawa K, Kitazume S, Oka R, Maruyama K, Saido TC, Sato Y, Endo T, Hashimoto Y. 2006. Sialylation enhances the secretion of neurotoxic amyloid-β peptides. *J Neurochem.* 96:924–933.

Narasimhan S. 1982. Control of glycoprotein synthesis. UDP-GlcNAc:glycopeptide β 4-*N*-acetylglucosaminyltransferase III, an enzyme in hen oviduct which adds GlcNAc in β 1–4 linkage to the beta-linked mannose of the trimannosyl core of *N*-glycosyl oligosaccharides. *J Biol Chem.* 257:10235–10242.

Nishikawa A, Ihara Y, Hatakeyama M, Kangawa K, Taniguchi N. 1992. Purification, cDNA cloning, and expression of UDP-*N*-acetylglucosamine: β-D-mannoside β-1,4*N*-acetylglucosaminyltransferase III from rat kidney. *J Biol Chem.* 267:18199–18204.

Ohtsubo K, Marth JD. 2006. Glycosylation in cellular mechanisms of health and disease. *Cell.* 126:855–867.

Pahlsson P, Shakin-Eshleman SH, Spitalnik SL. 1992. *N*-Linked glycosylation of β -amyloid precursor protein. *Biochem Biophys Res Commun.* 189:1667–1673.

Peiretti F, Canault M, Deprez-Beauclair P, Berthet V, Bonardo B, Juhan-Vague I, Nalbone G. 2003. Intracellular maturation and transport of tumor necrosis factor α converting enzyme. *Exp Cell Res.* 285:278–285.

Price DL, Sisodia SS, Borchelt DR. 1998. Genetic neurodegenerative diseases: The human illness and transgenic models. *Science.* 282:1079–1083.

Rebbaa A, Yamamoto H, Saito T, Meuillet E, Kim P, Kersey DS, Bremer EG, Taniguchi N, Moskal JR. 1997. Gene transfection-mediated overexpression of β 1,4-*N*-acetylglucosamine bisecting oligosaccharides in glioma cell line U373 MG inhibits epidermal growth factor receptor function. *J Biol Chem.* 272:9275–9279.

Rudd PM, Endo T, Colominas C, Groth D, Wheeler SF, Harvey DJ, Wormald MR, Serban H, Prusiner SB, Kobata A, et al. 1999. Glycosylation differences between the normal and pathogenic prion protein isoforms. *Proc Natl Acad Sci USA.* 96:13044–13049.

Saito F, Tani A, Miyatake T, Yanagisawa K. 1995. *N*-Linked oligosaccharide of β-amyloid precursor protein (β APP) of C6 glioma cells: Putative regulatory role in β APP processing. *Biochem Biophys Res Commun.* 210:703–710.

Sato Y, Liu C, Wojczyk BS, Kobata A, Spitalnik SL, Endo T. 1999. Study of the sugar chains of recombinant human amyloid precursor protein produced by Chinese hamster ovary cells. *Biochim Biophys Acta.* 1472:344–358.

Schachter H. 1986. Biosynthetic controls that determine the branching and microheterogeneity of protein-bound oligosaccharides. *Biochem Cell Biol.* 64:163–181.

Schachter H, Narasimhan S, Gleeson P, Vella G. 1983. Control of branching during the biosynthesis of asparagine-linked oligosaccharides. *Can J Biochem Cell Biol.* 61:1049–1066.

Schlondorff J, Becherer JD, Blobel CP. 2000. Intracellular maturation and localization of the tumour necrosis factor α convertase (TACE). *Biochem J.* 347(Pt 1):131–138.

Schmechel A, Strauss M, Schlicksupp A, Pipkorn R, Haass C, Bayer TA, Multhaup G. 2004. Human BACE forms dimers and colocalizes with APP. *J Biol Chem.* 279:39710–39717.

Shigeta M, Shibukawa Y, Ihara H, Miyoshi E, Taniguchi N, Gu J. 2006. β 1,4-*N*-acetylglucosaminyltransferase III potentiates β1 integrin-mediated neuritogenesis induced by serum deprivation in Neuro2a cells. *Glycobiology.* 16:564–571.

Sinha S, Lieberburg I. 1999. Cellular mechanisms of β-amyloid production and secretion. *Proc Natl Acad Sci USA.* 96:11049–11053.

Skovronsky DM, Fath S, Lee VM, Milla ME. 2001. Neuronal localization of the TNFα converting enzyme (TACE) in brain tissue and its correlation to amyloid plaques. *J Neurobiol.* 49:40–46.

Skovronsky DM, Moore DB, Milla ME, Doms RW, Lee VM. 2000. Protein kinase C-dependent α-secretase competes with β-secretase for cleavage of amyloid-β precursor protein in the trans-Golgi network. *J Biol Chem.* 275:2568–2575.

Suzuki N, Cheung TT, Cai XD, Odaka A, Otvos L Jr, Eckman C, Golde TE, Younkin SG. 1994. An increased percentage of long amyloid β protein secreted by familial amyloid β protein precursor (β APP717) mutants. *Science.* 264:1336–1340.

Taniguchi N, Nishikawa A, Fujii S, Gu JG. 1989. Glycosyltransferase assays using pyridylaminated acceptors: *N*-acetylglucosaminyltransferase III, IV, and V. *Methods Enzymol.* 179:397–408.

Thinakaran G, Borchelt DR, Lee MK, Slunt HH, Spitzer L, Kim G, Ratovitsky T, Davenport F, Nordstedt C, Seeger M, et al. 1996. Endoproteolysis of presenilin 1 and accumulation of processed derivatives in vivo. *Neuron.* 17:181–190.

Tomita S, Kirino Y, Suzuki T. 1998. Cleavage of Alzheimer's amyloid precursor protein (APP) by secretases occurs after *O*-glycosylation of APP in the protein secretory pathway. Identification of intracellular compartments in which APP cleavage occurs without using toxic agents that interfere with protein metabolism. *J Biol Chem.* 273:6277–6284.

Wang X, Inoue S, Gu J, Miyoshi E, Noda K, Li W, Mizuno-Horikawa Y, Nakano M, Asahi M, Takahashi M, et al. 2005. Dysregulation of TGF-β1 receptor activation leads to abnormal lung development and emphysema-like phenotype in core fucose-deficient mice. *Proc Natl Acad Sci USA.* 102:15791–15796.

Weidemann A, Konig G, Bunke D, Fischer P, Salbaum JM, Masters CL, Beyreuther K. 1989. Identification, biogenesis, and localization of precursors of Alzheimer's disease A4 amyloid protein. *Cell.* 57:115–126.

Wilson JR, Williams D, Schachter H. 1976. The control of glycoprotein synthesis: *N*-acetylglucosamine linkage to a mannose residue as a signal for the attachment of L-fucose to the asparagine-linked *N*-acetylglucosamine residue of glycopeptide from α1-acid glycoprotein. *Biochem Biophys Res Commun.* 72:909–916.

Yamashita K, Hitoi A, Kobata A. 1983. Structural determinants of Phaseolus vulgaris erythroagglutinating lectin for oligosaccharides. *J Biol Chem.* 258:14753–14755.

Yazaki M, Tagawa K, Maruyama K, Sorimachi H, Tsuchiya T, Ishiura S, Suzuki K. 1996. Mutation of potential *N*-linked glycosylation sites in the Alzheimer's disease amyloid precursor protein (APP). *Neurosci Lett.* 221:57–60.

Yoshimura M, Ihara Y, Matsuzawa Y, Taniguchi N. 1996. Aberrant glycosylation of E-cadherin enhances cell-cell binding to suppress metastasis. *J Biol Chem.* 271:13811–13815.

Eur J Nucl Med Mol Imaging
DOI 10.1007/s00259-009-1202-1

ORIGINAL ARTICLE

Validation of cardiac ^{123}I-MIBG scintigraphy in patients with Parkinson's disease who were diagnosed with dopamine PET

Kenji Ishibashi · Yuko Saito · Shigeo Murayama · Kazutomi Kanemaru · Keiichi Oda · Kiichi Ishiwata · Hidehiro Mizusawa · Kenji Ishii

Received: 11 March 2009 / Accepted: 9 June 2009

Abstract
Purpose The aim of this study was to evaluate the diagnostic potential of cardiac ^{123}I-labelled metaiodobenzylguanidine (^{123}I-MIBG) scintigraphy in idiopathic Parkinson's disease (PD). The diagnosis was confirmed by positron emission tomography (PET) imaging with ^{11}C-labelled 2β-carbomethoxy-3β-(4-fluorophenyl)-tropane (^{11}C-CFT) and ^{11}C-raclopride (together designated as dopamine PET).
Methods Cardiac ^{123}I-MIBG scintigraphy and dopamine PET were performed for 39 parkinsonian patients. To estimate the cardiac ^{123}I-MIBG uptake, heart to mediastinum (H/M) ratios in early and delayed images were calculated. On the basis of established clinical criteria and our dopamine PET findings, 24 patients were classified into the PD group and 15 into the non-PD (NPD) group.
Results Both early and delayed images showed that the H/M ratios were significantly lower in the PD group than in the NPD group. When the optimal cut-off levels of the H/M ratio were set at 1.95 and 1.60 in the early and delayed images, respectively, by receiver-operating characteristic analysis, the sensitivity of cardiac ^{123}I-MIBG scintigraphy for the diagnosis of PD was 79.2 and 70.8% and the specificity was 93.3 and 93.3% in the early and delayed images, respectively. In the Hoehn and Yahr 1 and 2 PD patients, the sensitivity decreased by 69.2 and 53.8% in the early and delayed images, respectively.
Conclusion In early PD cases, cardiac ^{123}I-MIBG scintigraphy is of limited value in the diagnosis, because of its relatively lower sensitivity. However, because of its high specificity for the overall cases, cardiac ^{123}I-MIBG scintigraphy may assist in the diagnosis of PD in a complementary role with the dopaminergic neuroimaging.

Keywords ^{123}I-MIBG · ^{11}C-CFT · ^{11}C-Raclopride · Scintigraphy · Positron emission tomography · Parkinson's disease

Introduction

Cardiac ^{123}I-labelled metaiodobenzylguanidine (^{123}I-MIBG) scintigraphy has been suggested to be useful for the diagnosis of idiopathic Parkinson's disease (PD), because many recent studies have revealed that cardiac ^{123}I-MIBG uptake decreases with disease progression and that almost all

An Editorial Commentary on this paper is available at http://dx.doi.org/10.1007/s00259-009-1215-9.

K. Ishibashi · H. Mizusawa
Department of Neurology and Neurological Science, Graduate School, Tokyo Medical and Dental University, Tokyo, Japan

K. Ishibashi · K. Oda · K. Ishiwata · K. Ishii (✉)
Positron Medical Center, Tokyo Metropolitan Institute of Gerontology, 1-1 Nakacho, Itabashi-ku, Tokyo 173-0022, Japan
e-mail: ishii@pet.tmig.or.jp

Y. Saito
Department of Pathology, Tokyo Metropolitan Geriatric Hospital, Tokyo, Japan

Y. Saito · S. Murayama
Department of Neuropathology, Tokyo Metropolitan Institute of Gerontology, Tokyo, Japan

K. Kanemaru
Department of Neurology, Tokyo Metropolitan Geriatric Hospital, Tokyo, Japan

Published online: 22 July 2009

patients in the advanced stage of PD show decreased cardiac ^{123}I-MIBG uptake [1–5]. However, it is unclear whether cardiac ^{123}I-MIBG uptake is a good surrogate marker for the diagnosis of PD, especially in early and mild PD cases, which are the most difficult to diagnose in daily clinical practice, because the data on the reduction of cardiac ^{123}I-MIBG uptake in the early stage of PD vary greatly among different studies [1–8]. Therefore, we aimed to investigate the sensitivity and specificity of cardiac ^{123}I-MIBG scintigraphy in diagnosing PD, focusing on early and mild cases of PD in the Hoehn and Yahr (HY) stages 1 and 2.

While planning this study, we focused on dividing the patients into PD and non-PD (NPD) groups in the most appropriate manner in order to acquire precise results. Previous studies have shown that the usual clinical diagnostic accuracy of PD ranges from 70 to 90%, and the accuracy rate greatly decreases in early cases [9–12]. In vivo neurofunctional imaging of the basal ganglia, which provides images of both pre- and postsynaptic nigrostriatal dopaminergic functions, has been recognized as a standard marker for the diagnosis of PD in every clinical stage [13–25]. Therefore, in order to improve the accuracy of the diagnosis of PD, especially in early PD cases, and to classify the patients into the PD and NPD groups in a more appropriate manner, we performed positron emission tomography (PET) imaging with ^{11}C-labelled 2β-carbomethoxy-3β-(4-fluorophenyl)-tropane (^{11}C-CFT) and ^{11}C-raclopride. PET imaging with ^{11}C-CFT and ^{11}C-raclopride can assess the levels of presynaptic dopamine transporter (DAT) and postsynaptic dopamine D_2-like receptor (D_2R), respectively, in the striatum. The two types of PET imaging techniques were together designated as dopamine PET. Further, we proposed the definitions of PD and NPD patterns in dopamine PET findings on the basis of the results which had been confirmed by previous studies.

We also investigated the association between cardiac sympathetic function assessed by cardiac ^{123}I-MIBG uptake, presynaptic nigrostriatal dopaminergic function assessed by striatal ^{11}C-CFT uptake and disease stage determined according to the HY scale.

Materials and methods

Subjects

The present study was a retrospective study. The subjects comprised 39 patients who visited the neurological outpatient clinic at Tokyo Metropolitan Geriatric Hospital from November 2001 to October 2007. They chiefly complained of one or more parkinsonian symptoms, including resting tremor, rigidity, bradykinesia and postural instability. The patients were divided into PD and NPD groups (Fig. 1). Cardiac ^{123}I-MIBG scintigraphy, dopamine PET and magnetic resonance imaging (MRI) were performed for all patients. None of the patients had any concomitant hereditary disorder that could cause parkinsonian symptoms. None of the patients had an individual history of any heart disease. Further, none of the patients were on any medication that could cause parkinsonian symptoms.

For dopamine PET, eight healthy subjects (five men and three women) aged 55–74 years [mean±standard deviation (SD) = 62.3±6.9 years)]were considered as controls. They were deemed healthy based on their medical history, physical and neurological examinations and MRI of the brain. Further, none of them were on medication.

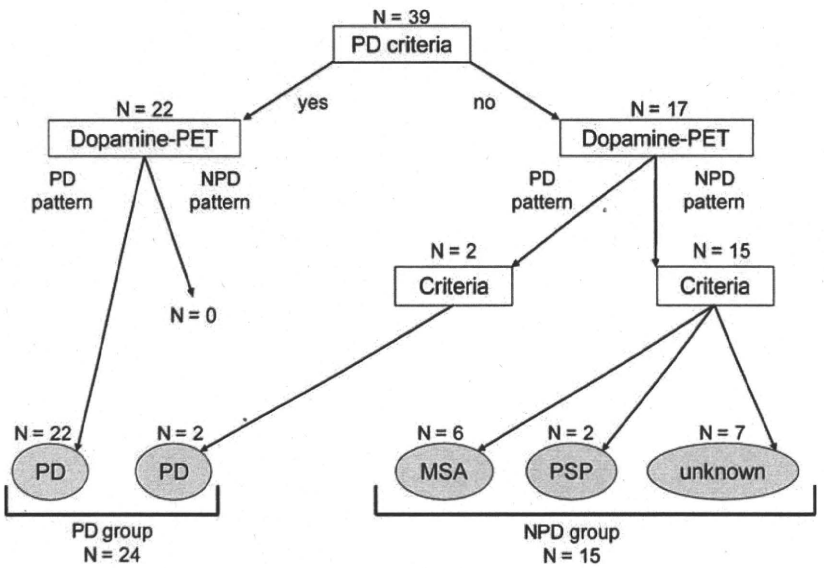

Fig. 1 Diagnostic flow chart and schematic representation of classification process. Patients were classified into PD and NPD groups on the basis of respective published clinical criteria and our dopamine PET findings

This study protocol was approved by the Ethics Committee of the Tokyo Metropolitan Institute of Gerontology. Written informed consent was obtained from all participants.

PET imaging

PET imaging was performed at the Positron Medical Center, Tokyo Metropolitan Institute of Gerontology by using a SET-2400 W scanner (Shimadzu, Kyoto, Japan) in the three-dimensional scanning mode [26], as described previously [27, 28]. The transmission data were acquired using a rotating ^{68}Ga/^{68}Ge rod source for attenuation correction. Images of 50 slices were obtained with a resolution of 2×2×3.125 mm voxels and a 128×128 matrix.

Dopamine PET imaging ^{11}C-CFT and ^{11}C-raclopride were prepared as described previously [29, 30]. The two types of PET imaging were performed for all of the subjects on the same day. The patients being treated with antiparkinsonian drugs underwent dopamine PET following at least 15 h deprivation of the medications. Each subject was administered an intravenous bolus injection of 341±62 (mean ± SD) MBq of ^{11}C-CFT, followed by that of 311±56 (mean ± SD) MBq of ^{11}C-raclopride after 2.5–3 h. To measure the uptake of the tracers, static scanning was performed for 75–90 and 40–55 min after the injection of ^{11}C-CFT and ^{11}C-raclopride, respectively. The specific activity of ^{11}C-CFT and ^{11}C-raclopride at the time of injection ranged from 5.9 to 134.2 GBq/μmol and from 10.2 to 201.7 GBq/μmol, respectively.

Analysis of dopamine PET images Image manipulations were performed using Dr. View version R2.0 (AJS, Tokyo, Japan) and SPM2 (Functional Imaging Laboratory, London, UK) implemented in MATLAB version 7.0.1 (The MathWorks, Natick, MA, USA).

The two PET images and one MRI image obtained for each subject were coregistered. The three coregistered images were resliced transaxially, parallel to the anteroposterior intercommissural (AC-PC) line. Circular regions of interest (ROIs) were selected with reference to the brain atlas and individually coregistered MRI images. In each of the three contiguous slices, one ROI with 8-mm diameter was selected on the caudate, two ROIs on the anterior putamen and two on the posterior putamen on both the left and right sides. In other words, the AC-PC plane and regions 3.1 and 6.2 mm above the AC-PC line were selected. A total of 50 ROIs with 10-mm diameter were selected throughout the cerebellar cortex in five contiguous slices.

To evaluate the uptake of ^{11}C-CFT and ^{11}C-raclopride, we calculated the uptake ratio index by the following formula [15, 31]: uptake ratio index = (activity in each region – activity in the cerebellum)/(activity in the cerebellum). We previously validated the method to estimate the binding potential of ^{11}C-raclopride and ^{11}C-CFT, adopting the uptake ratio index [27, 28]. For the further analyses, the uptake of each tracer in each subregion of the striatum (the caudate, anterior putamen and posterior putamen) was evaluated as the average value of the left and right sides. The uptake of each tracer in the whole striatum was evaluated as the average value of entire ROIs in the whole striatum.

Cardiac ^{123}I-MIBG scintigraphy

Scintigraphic studies were performed at Tokyo Metropolitan Geriatric Hospital by using a triple-headed gamma camera (PRISM-3000, Shimadzu, Kyoto, Japan). None of the patients were on any medication, i.e. they were not receiving any drugs such as antidepressants and monoamine oxidase inhibitors, which might influence cardiac ^{123}I-MIBG uptake. After a 30-min resting period, each patient was administered an intravenous bolus injection of 111 MBq of ^{123}I-MIBG (Fujifilm RI Pharma Co., Tokyo, Japan). Planar images of the chest in the anterior view were obtained twice for 5 min, starting at 20 min (early phase) and then at 180 min (delayed phase) after the injection of ^{123}I-MIBG. Relative organ uptake of ^{123}I-MIBG was determined by selecting the ROIs on the heart and mediastinum in the anterior planar image [32]. Average counts per pixel in the heart and mediastinum were used to calculate the heart to mediastinum (H/M) ratio.

MRI

MRI was performed at Tokyo Metropolitan Geriatric Hospital. By using a 1.5-T Signa EXCITE HD scanner (GE, Milwaukee, WI, USA), transaxial T1-weighted images [three-dimensional spoiled gradient-recalled (3D SPGR), repetition time (TR) = 9.2 ms, echo time (TE) = 2.0 ms, matrix size = 256 × 256 × 124, voxel size = 0.94 × 0.94 × 1.3mm] and transaxial T2-weighted images (first spin echo, TR= 3,000 ms, TE=100 ms, matrix size = 256 × 256 × 20, voxel size = 0.7 × 0.7 × 6.5mm) were obtained.

Clinical diagnosis

The diagnostic flow chart is shown in Fig. 1. First, the patients were divided into two groups (22 patients in one group and 17 patients in the other) on the basis of the clinical criteria of the UK Parkinson's Disease Brain Bank (UKPDBB) [10]. Each group was then further classified on the basis of dopamine PET findings. As shown in Fig. 2, the PD pattern in dopamine PET was defined as follows: (1)

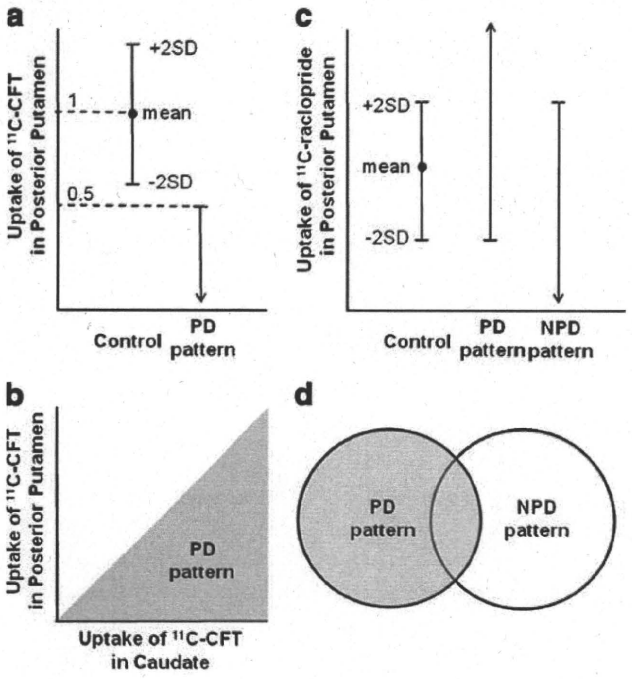

Fig. 2 PD and NPD patterns defined on the basis of dopamine PET findings. PD pattern: ^{11}C-CFT uptake in the posterior putamen of patients less than 50% of the mean uptake in the posterior putamen of normal controls (**a**) and less than that in the caudate of patients (**b**); ^{11}C-raclopride uptake in the posterior putamen of patients more than the mean – 2 SD of the uptake in the posterior putamen of normal controls (**c**). NPD pattern: ^{11}C-raclopride uptake in the posterior putamen of patients less than the mean + 2 SD of the uptake in the posterior putamen of normal controls (**c**). The patient was considered to be PD pattern when both PD and NPD were fulfilled (**d**). The uptake in each subregion of the striatum was evaluated as the average value of both sides

^{11}C-CFT uptake in the posterior putamen of the patients less than 50% of the mean uptake in the posterior putamen of normal controls (Fig. 2a) and less than that in the caudate of the patients (Fig. 2b) and (2) ^{11}C-raclopride uptake in the posterior putamen of the patients more than the mean – 2 SD of the uptake in the posterior putamen of normal controls (Fig. 2c). The NPD pattern was defined as follows: ^{11}C-raclopride uptake in the posterior putamen of the patients less than the mean + 2 SD of the uptake in the posterior putamen of normal controls (Fig. 2c). The patient was considered to be PD pattern when both PD and NPD were fulfilled (Fig. 2d).

Statistical analysis

Differences in the averages and variances were tested by Student's t test and one-way analysis of variance, respectively. Correlations between the two groups of patients were assessed by linear regression analysis with Pearson's correlation test; p values of <0.05 were considered statistically significant.

Results

Patients

Classification into PD and NPD groups All 22 patients who fulfilled the UKPDBB PD criteria at initial diagnosis [10] showed the PD pattern on dopamine PET (Fig. 1). They were classified into the PD group. The other 17 patients were further classified according to dopamine PET findings and respective published clinical criteria. Of the 17 patients, 2 showed the PD pattern on dopamine PET. In fact, the symptom manifested was only resting tremor at initial diagnosis; however, during the course of the study, they fulfilled the UKPDBB PD criteria [10] and were classified into the PD group.

Of the 17 patients, 15 showed the NPD pattern on dopamine PET and were classified into the NPD group (Fig. 1). These patients were then further divided into three subgroups. Six patients fulfilled the multiple system atrophy (MSA) criteria [33]. Two patients fulfilled the progressive supranuclear palsy (PSP) criteria [34]. For the remaining seven patients, no definitive diagnoses could be established despite follow-up for more than 1 year.

Finally, 24 patients (7 men and 17 women, age range: 60–85 years, mean age ± SD = 71.5±6.8 years) and 15 patients (8 men and 7 women, age range: 65–86 years, mean age ± SD: 76.0±5.5 years) were classified into the PD and NPD groups, respectively.

Demographic data Patient characteristics are summarized in Table 1. In the PD group, 11 patients were drug naive, 7 were being treated with L-dopa and 6 were being treated with L-dopa and dopamine agonists at the time of dopamine PET. The interval between cardiac ^{123}I-MIBG scintigraphy and dopamine PET was within 6 months for 16 patients, between 6 and 12 months for 1 patient and more than 1 year for 7 patients. However, the HY stage of each patient in the PD group remained the same between cardiac ^{123}I-MIBG scintigraphy and dopamine PET. In the NPD group, 11 patients were not administered any antiparkinsonian drug, and 4 were being treated with only L-dopa. The interval between the two examinations was within 6 months for 12 patients, between 6 and 12 months for 1 patient and more than 1 year for 2 patients.

Uptake of ^{123}I-MIBG

Both the early and delayed images showed significantly lower H/M ratios in the PD group than in the NPD group (Fig. 3). In both the early and delayed images, the H/M ratios tended to decrease with the progression of the HY stages; however, the decrease was not statistically significant.

Table 1 Clinical features of patients in Parkinson's disease and non-Parkinson's disease groups

Groups	Patients		Age (years)	Duration (years)	^{123}I-MIBG scintigraphy		^{11}C-CFT PET
	Number	M:F			Heart to mediastinum ratio		Uptake ratio index in the whole striatum
					Early	Delayed	
Parkinson's disease	24	7:17	71.5±6.8	3.5±3.2	1.66±0.45	1.46±0.41	0.98±0.34
Hoehn and Yahr 1	4	0:4	65.0±7.7	2.9±2.6	1.75±0.33	1.49±0.29	1.49±0.40
Hoehn and Yahr 2	9	2:7	73.9±5.6	2.4±1.0	1.81±0.54	1.60±0.45	1.00±0.20
Hoehn and Yahr 3	8	5:3	71.9±7.2	3.0±1.8	1.57±0.44	1.41±0.44	0.81±0.20
Hoehn and Yahr 4	3	0:3	72.3±5.0	9.0±6.1	1.36±0.05	1.12±0.08	0.69±0.07
Non-Parkinson's disease	15	8:7	76.0±5.5	2.8±1.9	2.35±0.46	2.18±0.51	1.65±0.68

Data are expressed as mean±SD

Table 2 shows the sensitivity and specificity of cardiac ^{123}I-MIBG scintigraphy in differentiating patients with PD from the other patients with chief complaints of parkinsonian symptoms. When the optimal cut-off levels of ^{123}I-MIBG were set at 1.95 and 1.60 by receiver-operating characteristic analysis, the sensitivity of cardiac ^{123}I-MIBG scintigraphy for the diagnosis of PD was 79.2 and 70.8% and the specificity was 93.3 and 93.3% in the early image and delayed images, respectively. In HY 1 and 2 PD patients the sensitivity was 69.2 and 53.9% and in HY 3 and 4 PD patients the sensitivity was 90.9 and 90.9% in the early image and delayed images, respectively

Uptake of ^{11}C-CFT

The uptake of ^{11}C-CFT in the whole striatum decreased with the progression of the HY stages (Fig. 4). Significant reduction in the ^{11}C-CFT uptake with the progression of the HY stages was also observed in each of the three subregions of the striatum. Correlation between cardiac ^{123}I-MIBG scintigraphy and ^{11}C-CFT PET was evaluated in the 16 patients who underwent the two examinations within 6 months. There was no significant correlation between the ^{11}C-CFT uptake in the whole striatum and the H/M ratios in both the early images (r=0.15, p=0.59) and delayed images (r=0.21, p=0.43) (Fig. 5). Further, no significant correlation was observed between the ^{11}C-CFT uptake in each of the three subregions of the striatum and the H/M ratio.

Discussion

In the present study, we investigated the sensitivity and specificity of cardiac ^{123}I-MIBG scintigraphy in diagnosing PD and differentiating the patients with PD from the others with chief complaints of parkinsonian symptoms. Further, we investigated the correlation between cardiac sympathetic function assessed by cardiac ^{123}I-MIBG uptake, nigrostriatal

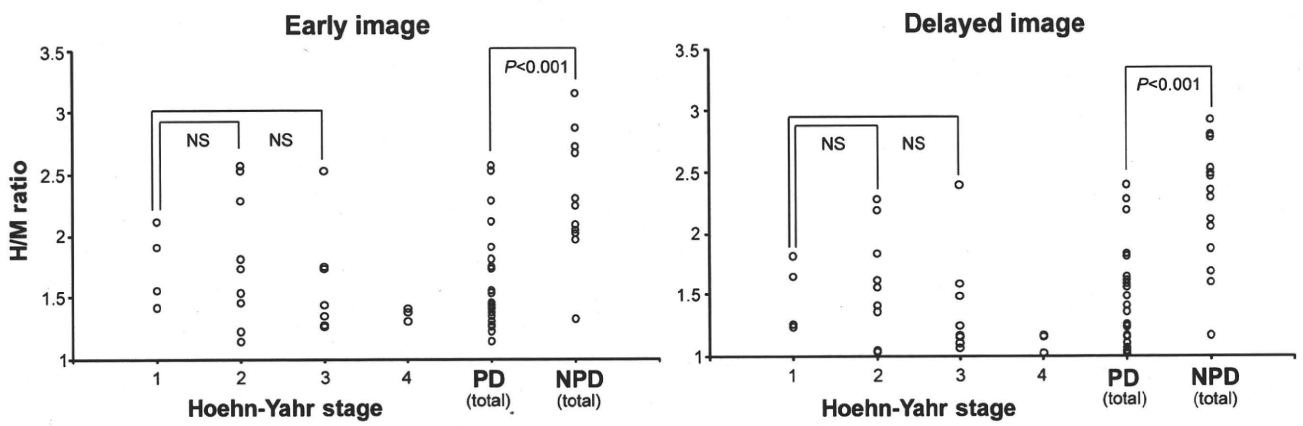

Fig. 3 H/M ratios in the PD and NPD groups in early and delayed images. Each graph represents the relation between the H/M ratio and Hoehn and Yahr stage of PD and a comparison of the H/M ratios of the total number of PD and NPD patients. Both images showed that the H/M ratios were significantly lower in the PD group than in the NPD group; however, the H/M ratios of patients in HY 1 of PD were not significantly higher than those of the patients in HY 2 and 3 of PD. *NS* not significant

Table 2 Sensitivity and specificity of cardiac ^{123}I-MIBG scintigraphy in differentiating Parkinson's disease from other parkinsonian syndromes

Total PD patients (n=24)												
	Early image						Delayed image					
Cut-off	1.80	1.85	1.90	1.95	2.00	2.05	1.60	1.65	1.70	1.75	1.80	1.85
Sensitivity	70.8%	75.0%	75.0%	79.2%	79.2%	79.2%	70.8%	75.0%	79.2%	79.2%	79.2%	87.5%
Specificity	93.3%	93.3%	93.3%	93.3%	86.7%	80.0%	93.3%	80.0%	73.3%	73.3%	73.3%	73.3%
Hoehn and Yahr 1 and 2 (n=15)												
	Early image						Delayed image					
Cut-off	1.80	1.85	1.90	1.95	2.00	2.05	1.60	1.65	1.70	1.75	1.80	1.85
Sensitivity	53.8%	61.5%	61.5%	69.2%	69.2%	69.2%	53.8%	61.5%	69.2%	69.2%	69.2%	84.6%

Cut-off levels, for which both the sensitivity and specificity were more than 70%, are shown. The optimal cut-off levels determined by receiver-operating characteristic analysis were at 1.95 and 1.60 in the early and delayed images, respectively

dopaminergic function assessed by ^{11}C-CFT uptake and disease stage determined according to the HY scale.

It has been reported that cardiac ^{123}I-MIBG uptake in patients with PD is significantly lower than that in patients with other parkinsonian syndromes [1–7]; this result corresponds to our results. Several reports suggest that the severity of motor impairment and disease duration are correlated with reduced ^{123}I-MIBG uptake in patients with PD [1, 2, 5, 6]; however, some other findings deny such correlations, similar to ours [3, 4, 7, 8]. This discrepancy is presumably explained by the fact that the degree of cardiac ^{123}I-MIBG uptake in patients in HY 1 and 2 of PD varies greatly among different studies. Difficult definitive diagnosis of PD in early and mild cases may also be because of the great variation. On the other hand, almost all patients in the advanced stage of PD have shown very low ^{123}I-MIBG uptake in both the previous and the present studies. Li et al. reported that cardiac sympathetic denervation progresses over time and that the rate of decrease in the number of sympathetic terminals appears to be at least as high as that of nigrostriatal dopaminergic terminals [35]. Therefore, we considered that although the onset of cardiac sympathetic denervation varied among the patients with PD, severe cardiac sympathetic denervation occurred in all of the patients by the terminal stage of PD. In regard to the association with a sympathetic symptom, it was reported that reduced ^{123}I-MIBG uptake does not always mean the existence of a sympathetic symptom [1, 3, 4, 7]. Also in this study, of the three patients in stage 4 of the HY scale who showed very low ^{123}I-MIBG uptake (Fig. 3), two had orthostatic hypotension; however, the remaining one patient had no cardiovascular sympathetic symptom and showed no abnormality in the head-up tilt test. In contrast to ^{123}I-MIBG uptake, the decrease in ^{11}C-CFT uptake in the whole striatum and in each of its three subregions significantly correlated with disease progression represented by the HY stages, as reported previously [14, 16, 22]. Considering the causal pathophysiological mechanism of PD, this is reasonable because ^{11}C-CFT uptake directly indicates nigrostriatal dopaminergic function.

We investigated the sensitivity and specificity of cardiac ^{123}I-MIBG scintigraphy in diagnosing PD and differentiating the patients with PD from the other patients with chief complaints of parkinsonian symptoms. Similar to the

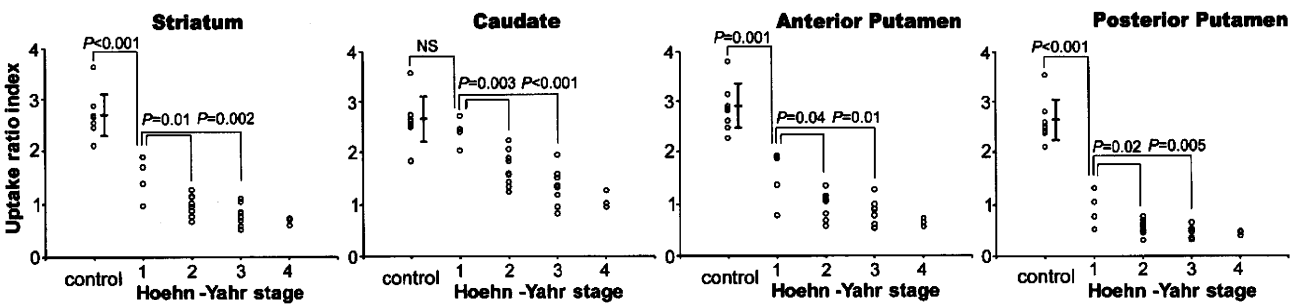

Fig. 4 Relation between the HY stage and uptake ratio index of ^{11}C-CFT in the whole striatum, caudate, anterior putamen and posterior putamen of patients with PD. In all four graphs, the uptakes in the patients in HY 1 of PD are significantly higher than those in the patients in HY 2 and 3 of PD. The uptakes in the caudate of patients in HY 1 of PD are not significantly higher than those in the caudate of controls, while the uptakes in the whole striatum, anterior putamen and posterior putamen of patients in HY 1 of PD are significantly higher than those in the corresponding regions of the controls. The *vertical bar* represents the mean ± SD of controls. *NS* not significant

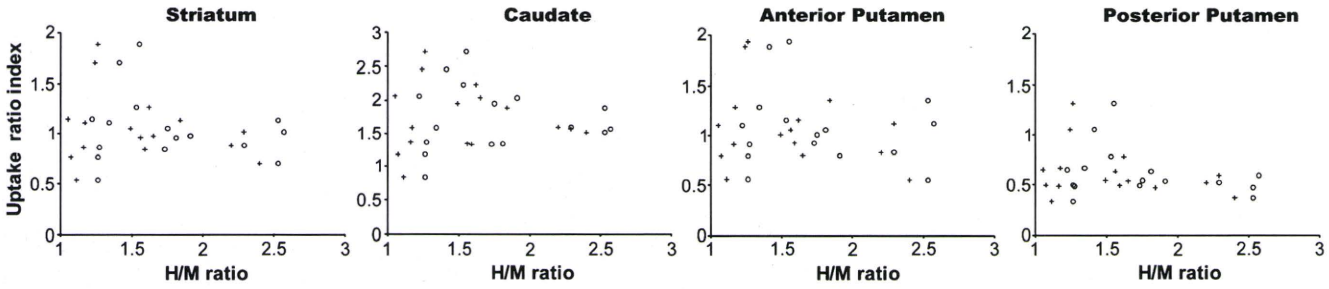

Fig. 5 Relation between the H/M ratio and uptake ratio index of ^{11}C-CFT in the whole striatum, caudate, anterior putamen and posterior putamen of patients with PD. Correlation was evaluated for 16 patients who underwent the two examinations (scintigraphy and PET) within 6 months. In all four graphs, no significant correlations are observed between the early images (*open circles*) and delayed images (*plus signs*)

previous meta-analysis of studies with a total of 246 PD cases [36], in both early and delayed images our study showed high specificity for the overall cases and high sensitivity for the advanced cases. However, early cases tended to have relatively lower sensitivity in both images, although the sample size and methodology greatly differed among the studies. Thus, our results suggested that even in the case of sustained cardiac ^{123}I-MIBG uptake, the possibility of PD should not be denied and follow-up clinical examinations, including ^{123}I-MIBG scintigraphy, should be conducted, especially in early and mild PD cases.

No definite correlation was found either between cardiac ^{123}I-MIBG uptake and striatal ^{11}C-CFT uptake or between cardiac ^{123}I-MIBG uptake and subregional ^{11}C-CFT uptake in the PD group. Two groups have reported the association between the functional impairment of the nigrostriatal dopaminergic system and that of the cardiac sympathetic system [8, 37]. Spiegel et al. (n=18) found a correlation between the two indices, i.e. ^{123}I-MIBG and ^{11}C-CFT uptake, while Raffel et al. (n=9) found no correlation between them. This discrepancy may be explained as follows. The functional impairment of both the nigrostriatal dopaminergic and cardiac sympathetic systems increases with disease progression, as described earlier; hence, a correlation was observed in some studies. On the other hand, there is no report that suggests a direct cause-effect relationship between the functional impairment of the nigrostriatal dopaminergic system and that of the cardiac sympathetic system. Thus, a statistically significant correlation between the functional impairments of the two systems may depend on the sample size and methodology. However, the functional impairments of the two systems would, in fact, occur and progress independently. Sometimes, impairment of the cardiac sympathetic function may precede that of the nigrostriatal dopaminergic function, while at other times, the latter may precede the former.

This is the first report wherein PD and NPD patterns in dopamine PET findings were defined on the basis of the results which have been confirmed as follows. In presynaptic DAT images, three characteristic changes are observed [14–16, 22]. First, the reduction in the ^{11}C-CFT uptake in the striatum begins from the posterior putamen, representing the initial locus of PD [38]. Second, the uptake ratio of the posterior putamen to the caudate is less than 1. Third, one putamen is usually more affected than the other, reflecting asymmetric degeneration. In fact, Fig. 4 shows that the ^{11}C-CFT uptake in the posterior putamen markedly decreased in the early stage of PD, while that in the caudate was relatively constant in the early stage. In postsynaptic D_2R images, putaminal uptake is normal or mildly upregulated in untreated PD, presumably as a compensatory response to decrease in presynaptic dopamine [17–19]. On the other hand, in treated or longstanding PD, the uptake restores to the normal level in the putamen and most often decreases in the caudate; this is presumably as a result of long-term downregulation due to chronic dopaminergic therapy or structural adaptation of the postsynaptic dopaminergic system to the progressive degeneration of nigrostriatal neurons [17, 19, 21]. In fact, in vitro studies have reported that the densities of striatal D_2Rs are maintained even in the advanced stage [39, 40].

On the basis of the earlier mentioned characteristic changes, especially in the posterior putamen, we defined the PD and NPD patterns such that false-negative cases should be as few as possible, because the aim was to reinforce the published clinical criteria. For defining the PD pattern, we considered that ^{11}C-CFT uptake in the posterior putamen of the patients should be less than that in the caudate of the patients and less than 50% of the mean uptake in normal controls. This percentage (i.e. 50%) was selected (1) on the basis of previous PET reports and considered suitable to distinguish normal from affected individuals [14–16, 22] and (2) on the basis of previous reports of in vitro studies, stating that parkinsonian symptoms appear when 80% of the striatal dopamine is lost or 50% of the nigral cells degenerate [38, 41]. Asymmetric uptake was not defined because of the difficulty in determining the intraindividual differences in

the uptake on the left and right sides. However, all 24 patients with PD showed asymmetric uptake. In the ^{11}C-raclopride PET image, since the uptake in the putamen was not less than the normal range, we considered that the uptake in the posterior putamen was normal or increased. For defining the NPD pattern, presynaptic function was not determined because the degree of the presynaptic dysfunction varies with diseases. In the ^{11}C-raclopride PET image, we considered that the uptake in the posterior putamen was normal or decreased because the uptake was not more than the normal range, except for Lewy body disease.

Conclusions

In early and mild PD cases, cardiac ^{123}I-MIBG scintigraphy is of limited value in the diagnosis of PD, because the sensitivity was indicated to be less than 70%. However, because of its high specificity for the overall cases and high sensitivity for the advanced cases, cardiac ^{123}I-MIBG scintigraphy may assist in the diagnosis of PD in a complementary role with the dopaminergic neuroimaging. Disease progression indicated by the HY stages has a stronger association with the nigrostriatal dopaminergic function assessed by striatal ^{11}C-CFT uptake than with the cardiac sympathetic function assessed by cardiac ^{123}I-MIBG uptake. The impairment of the two functions would occur and progress independently.

Acknowledgments The authors thank Mr. Keiichi Kawasaki, Dr. Masaya Hashimoto, and Ms. Hiroko Tsukinari for their technical assistance and useful discussions. This work was supported by grant-in-aid for Scientific Research (B) No. 20390334 (Ki.I.) from the Japan Society for the Promotion of Science and a grant (06-46) (Ki.I.) from the Program for Promotion of Fundamental Studies in Health Sciences of the National Institute of Biomedical Innovation of Japan, and a grant-in-aid for Neurological and Psychiatric Research (S.M., Y.S., and Ke.I.), and Research fo Longevity (S.M., Y.S., and Ke.I.) from the Ministry of Health, Labor, and Welfare of Japan, a grant-in-aid for Long-Term Comprehensive Research on Age-associated Dementia from the Tokyo Metropolitan Institute of Gerontology (K.K., S.M., and Ke.I.).

References

1. Orimo S, Ozawa E, Nakade S, Sugimoto T, Mizusawa H. (123)I-metaiodobenzylguanidine myocardial scintigraphy in Parkinson's disease. J Neurol Neurosurg Psychiatry 1999;67:189–94.
2. Satoh A, Serita T, Seto M, Tomita I, Satoh H, Iwanaga K, et al. Loss of 123I-MIBG uptake by the heart in Parkinson's disease: assessment of cardiac sympathetic denervation and diagnostic value. J Nucl Med 1999;40:371–5.
3. Taki J, Nakajima K, Hwang EH, Matsunari I, Komai K, Yoshita M, et al. Peripheral sympathetic dysfunction in patients with Parkinson's disease without autonomic failure is heart selective and disease specific. taki@med.kanazawa-u.ac.jp. Eur J Nucl Med 2000;27:566–73.
4. Takatsu H, Nishida H, Matsuo H, Watanabe S, Nagashima K, Wada H, et al. Cardiac sympathetic denervation from the early stage of Parkinson's disease: clinical and experimental studies with radiolabeled MIBG. J Nucl Med 2000;41:71–7.
5. Nagayama H, Hamamoto M, Ueda M, Nagashima J, Katayama Y. Reliability of MIBG myocardial scintigraphy in the diagnosis of Parkinson's disease. J Neurol Neurosurg Psychiatry 2005;76:249–51.
6. Hamada K, Hirayama M, Watanabe H, Kobayashi R, Ito H, Ieda T, et al. Onset age and severity of motor impairment are associated with reduction of myocardial 123I-MIBG uptake in Parkinson's disease. J Neurol Neurosurg Psychiatry 2003;74:423–6.
7. Braune S, Reinhardt M, Schnitzer R, Riedel A, Lucking CH. Cardiac uptake of [123I]MIBG separates Parkinson's disease from multiple system atrophy. Neurology 1999;53:1020–5.
8. Raffel DM, Koeppe RA, Little R, Wang CN, Liu S, Junck L, et al. PET measurement of cardiac and nigrostriatal denervation in Parkinsonian syndromes. J Nucl Med 2006;47:1769–77.
9. Rajput AH, Rozdilsky B, Rajput A. Accuracy of clinical diagnosis in parkinsonism–a prospective study. Can J Neurol Sci 1991;18:275–8.
10. Hughes AJ, Daniel SE, Kilford L, Lees AJ. Accuracy of clinical diagnosis of idiopathic Parkinson's disease: a clinico-pathological study of 100 cases. J Neurol Neurosurg Psychiatry 1992;55:181–4.
11. Jankovic J, Rajput AH, McDermott MP, Perl DP. The evolution of diagnosis in early Parkinson disease. Parkinson Study Group. Arch Neurol 2000;57:369–72.
12. Hughes AJ, Daniel SE, Lees AJ. Improved accuracy of clinical diagnosis of Lewy body Parkinson's disease. Neurology 2001;57:1497–9.
13. Plotkin M, Amthauer H, Klaffke S, Kuhn A, Ludemann L, Arnold G, et al. Combined 123I-FP-CIT and 123I-IBZM SPECT for the diagnosis of parkinsonian syndromes: study on 72 patients. J Neural Transm 2005;112:677–92.
14. Nurmi E, Bergman J, Eskola O, Solin O, Vahlberg T, Sonninen P, et al. Progression of dopaminergic hypofunction in striatal subregions in Parkinson's disease using [18F]CFT PET. Synapse 2003;48:109–15.
15. Frost JJ, Rosier AJ, Reich SG, Smith JS, Ehlers MD, Snyder SH, et al. Positron emission tomographic imaging of the dopamine transporter with 11C-WIN 35,428 reveals marked declines in mild Parkinson's disease. Ann Neurol 1993;34:423–31.
16. Rinne JO, Ruottinen H, Bergman J, Haaparanta M, Sonninen P, Solin O. Usefulness of a dopamine transporter PET ligand [(18)F] beta-CFT in assessing disability in Parkinson's disease. J Neurol Neurosurg Psychiatry 1999;67:737–41.
17. Antonini A, Schwarz J, Oertel WH, Beer HF, Madeja UD, Leenders KL. [11C]raclopride and positron emission tomography in previously untreated patients with Parkinson's disease: influence of L-dopa and lisuride therapy on striatal dopamine D2-receptors. Neurology 1994;44:1325–9.
18. Kaasinen V, Ruottinen HM, Någren K, Lehikoinen P, Oikonen V, Rinne JO. Upregulation of putaminal dopamine D2 receptors in early Parkinson's disease: a comparative PET study with [11C] raclopride and [11C]N-methylspiperone. J Nucl Med 2000;41:65–70.
19. Rinne JO, Laihinen A, Rinne UK, Någren K, Bergman J, Ruotsalainen U. PET study on striatal dopamine D2 receptor changes during the progression of early Parkinson's disease. Mov Disord 1993;8:134–8.
20. Dentresangle C, Veyre L, Le Bars D, Pierre C, Lavenne F, Pollak P, et al. Striatal D2 dopamine receptor status in Parkinson's disease: an [18F]dopa and [11C]raclopride PET study. Mov Disord 1999;14:1025–30.
21. Antonini A, Schwarz J, Oertel WH, Pogarell O, Leenders KL. Long-term changes of striatal dopamine D2 receptors in patients

with Parkinson's disease: a study with positron emission tomography and [11C]raclopride. Mov Disord 1997;12:33–8.
22. Wang J, Zuo CT, Jiang YP, Guan YH, Chen ZP, Xiang JD, et al. 18F-FP-CIT PET imaging and SPM analysis of dopamine transporters in Parkinson's disease in various Hoehn & Yahr stages. J Neurol 2007;254:185–90.
23. Knudsen GM, Karlsborg M, Thomsen G, Krabbe K, Regeur L, Nygaard T, et al. Imaging of dopamine transporters and D2 receptors in patients with Parkinson's disease and multiple system atrophy. Eur J Nucl Med Mol Imaging 2004;31:1631–8.
24. Kim YJ, Ichise M, Ballinger JR, Vines D, Erami SS, Tatschida T, et al. Combination of dopamine transporter and D2 receptor SPECT in the diagnostic evaluation of PD, MSA, and PSP. Mov Disord 2002;17:303–12.
25. Verstappen CC, Bloem BR, Haaxma CA, Oyen WJ, Horstink MW. Diagnostic value of asymmetric striatal D2 receptor upregulation in Parkinson's disease: an [123I]IBZM and [123I]FP-CIT SPECT study. Eur J Nucl Med Mol Imaging 2007;34:502–7.
26. Fujiwara T, Watanuki S, Yamamoto S, Miyake M, Seo S, Itoh M, et al. Performance evaluation of a large axial field-of-view PET scanner: SET-2400W. Ann Nucl Med 1997;11:307–13.
27. Hashimoto M, Kawasaki K, Suzuki M, Mitani K, Murayama S, Mishina M, et al. Presynaptic and postsynaptic nigrostriatal dopaminergic functions in multiple system atrophy. Neuroreport 2008;19:145–50.
28. Ishibashi K, Ishii K, Oda K, Kawasaki K, Mizusawa H, Ishiwata K. Regional analysis of age-related decline in dopamine transporters and dopamine D2-like receptors in human striatum. Synapse 2009;63:282–90.
29. NK LO, Dolle F, Lundkvist C, Sandell J, Swahn CG, Vaufrey F, et al. Precursor synthesis and radiolabelling of the dopamine D2 receptor ligand [11C]raclopride from [11C]methyl triflate. J Labelled Compd Radiopharm 1999;42:1183–93.
30. Kawamura K, Oda K, Ishiwata K. Age-related changes of the [11C]CFT binding to the striatal dopamine transporters in the Fischer 344 rats: a PET study. Ann Nucl Med 2003;17:249–53.
31. Antonini A, Leenders KL, Reist H, Thomann R, Beer HF, Locher J. Effect of age on D2 dopamine receptors in normal human brain measured by positron emission tomography and 11C-raclopride. Arch Neurol 1993;50:474–80.
32. Nakajima K, Taki J, Tonami N, Hisada K. Decreased 123I-MIBG uptake and increased clearance in various cardiac diseases. Nucl Med Commun 1994;15:317–23.
33. Gilman S, Low PA, Quinn N, Albanese A, Ben-Shlomo Y, Fowler CJ, et al. Consensus statement on the diagnosis of multiple system atrophy. J Auton Nerv Syst 1998;74:189–92.
34. Litvan I, Agid Y, Calne D, Campbell G, Dubois B, Duvoisin RC, et al. Clinical research criteria for the diagnosis of progressive supranuclear palsy (Steele-Richardson-Olszewski syndrome): report of the NINDS-SPSP international workshop. Neurology 1996;47:1–9.
35. Li ST, Dendi R, Holmes C, Goldstein DS. Progressive loss of cardiac sympathetic innervation in Parkinson's disease. Ann Neurol 2002;52:220–3.
36. Braune S. The role of cardiac metaiodobenzylguanidine uptake in the differential diagnosis of parkinsonian syndromes. Clin Auton Res 2001;11:351–5.
37. Spiegel J, Mollers MO, Jost WH, Fuss G, Samnick S, Dillmann U, et al. FP-CIT and MIBG scintigraphy in early Parkinson's disease. Mov Disord 2005;20:552–61.
38. Fearnley JM, Lees AJ. Ageing and Parkinson's disease: substantia nigra regional selectivity. Brain 1991;114(Pt 5):2283–301.
39. Guttman M, Seeman P, Reynolds GP, Riederer P, Jellinger K, Tourtellotte WW. Dopamine D2 receptor density remains constant in treated Parkinson's disease. Ann Neurol 1986;19:487–92.
40. Bokobza B, Ruberg M, Scatton B, Javoy-Agid F, Agid Y. [3H] spiperone binding, dopamine and HVA concentrations in Parkinson's disease and supranuclear palsy. Eur J Pharmacol 1984;99:167–75.
41. Kish SJ, Shannak K, Hornykiewicz O. Uneven pattern of dopamine loss in the striatum of patients with idiopathic Parkinson's disease. Pathophysiologic and clinical implications. N Engl J Med 1988;318:876–80.

Acta Neurol Scand DOI: 10.1111/j.1600-0404.2009.01255.x

ACTA NEUROLOGICA
SCANDINAVICA

Cerebrospinal fluid metabolite and nigrostriatal dopaminergic function in Parkinson's disease

Ishibashi K, Kanemaru K, Saito Y, Murayama S, Oda K, Ishiwata K, Mizusawa H, Ishii K. Cerebrospinal fluid metabolite and nigrostriatal dopaminergic function in Parkinson's disease.
Acta Neurol Scand: DOI: 10.1111/j.1600-0404.2009.01255.x.

Objectives – To evaluate the association between cerebrospinal fluid (CSF) homovanillic acid (HVA) concentrations and nigrostriatal dopaminergic function assessed by positron emission tomography (PET) imaging with carbon-11-labeled 2β-carbomethoxy-3β-(4-fluorophenyl)-tropane (^{11}C-CFT), which can measure the dopamine transporter (DAT) density, in Parkinson's disease (PD). *Methods* – ^{11}C-CFT PET scans and CSF examinations were performed on 21 patients with PD, and six patients with non-parkinsonian syndromes (NPS) as a control group. *Results* – In the PD group, CSF HVA concentrations were significantly correlated with the striatal uptake of ^{11}C-CFT ($r = 0.76$, $P < 0.01$). However, in the NPS group, two indices were within the normal range. *Conclusions* – In PD, CSF HVA concentrations correlate with nigrostriatal dopaminergic function. Therefore, CSF HVA concentrations may be an additional surrogate marker for estimating the remaining nigrostriatal dopaminergic function in case that DAT imaging is unavailable.

K. Ishibashi[1,2], K. Kanemaru[3], Y. Saito[4], S. Murayama[5], K. Oda[2], K. Ishiwata[2], H. Mizusawa[1], K. Ishii[2]

[1]Department of Neurology and Neurological Science, Graduate School, Tokyo Medical and Dental University, Tokyo, Japan; [2]Positron Medical Center, Tokyo Metropolitan Institute of Gerontology, Tokyo, Japan; [3]Department of Neurology, Tokyo Metropolitan Geriatric Hospital, Tokyo, Japan; [4]Department of Pathology, Tokyo Metropolitan Geriatric Hospital, Tokyo, Japan; [5]Department of Neuropathology, Tokyo Metropolitan Institute of Gerontology, Tokyo, Japan

Key words: cerebrospinal fluid; dopamine transporter; homovanillic acid; Parkinson's disease; positron emission tomography; ^{11}C-CFT

Kenji Ishii, MD, Positron Medical Center, Tokyo Metropolitan Institute of Gerontology, 1-1 Nakacho, Itabashi-ku, Tokyo 173-0022, Japan
Tel.: +81 3 3964 3241
Fax: +81 3 3964 2188
e-mail: ishii@pet.tmig.or.jp

Accepted for publication June 25, 2009

Introduction

In humans, homovanillic acid (HVA) is the major end-product of dopamine metabolism. The HVA in the cerebrospinal fluid (CSF) is largely derived from the nigrostriatal dopaminergic pathway; therefore, HVA concentration in the CSF has been used as an index of dopamine synthesis and presumed to reflect nigrostriatal dopaminergic function. However, even with the availability of a rigorous collection protocol, especially with respect to puncture time and pre-procedural resting, considerable inter-individual and intra-individual variability has been reported with regard to the concentration of CSF HVA in subjects with normal nigrostriatal function (1–3). Therefore, the extent to which CSF HVA concentrations reflect the nigrostriatal dopaminergic function is still unknown, and no study has specifically elucidated the association between the concentration of CSF HVA and the function of nigrostriatal dopamine.

Many studies have shown that the concentration of CSF HVA substantially reduces in patients with Parkinson's disease (PD), which is a neurodegenerative disorder caused by nigrostriatal dopaminergic dysfunction (4–12). However, the extent of reduction also varied a great deal among patients with PD. Because of the variability, the relationship of clinical disability with CSF HVA concentrations and the accuracy of CSF HVA concentrations in differentiating PD from other parkinsonian syndromes have yet to be determined. Several authors have reported an inverse relationship between CSF HVA concentrations and the clinical severity (5–7, 10, 11), while others have denied such a relationship (9, 12, 13). Other neurodegenerative disorders caused by the dysfunction of nigrostriatal dopaminergic system, such as multiple system atrophy (MSA), progressive

supranuclear palsy (PSP) and corticobasal degeneration, also show the reductions of CSF HVA concentrations as compared to normal subjects (8, 14, 15). Therefore, the usefulness of measuring CSF HVA concentrations in daily clinical practice has not yet been established.

In order to address the physiological and pathophysiological backgrounds of these issues, we evaluated the correlation between CSF HVA concentrations and nigrostriatal dopaminergic function. Furthermore, we have discussed the mechanism by which the concentration of CSF HVA reduces in patients with PD.

As means of evaluating nigrostriatal dopaminergic function, we performed carbon-11-labeled 2β-carbomethoxy-3β-(4-fluorophenyl)-tropane (^{11}C-CFT) positron emission tomography (PET) scans which can reveal the dopamine transporter (DAT) density in the striatum. DAT imaging has been recognized as a standard marker for the diagnosis of PD, because it is a very sensitive, reproducible, and reliable marker of nigrostriatal dopaminergic function (16–21).

Materials and methods

Subjects

The present study was a retrospective study. The subjects comprised 35 patients [19 men and 16 women; age 60–83 years (mean age = 71.7 years, SD = 6.0)]. They visited the neurological outpatient clinic at Tokyo Metropolitan Geriatric Hospital from April 2001–November 2004. Of the 35 patients, 29 had parkinsonian symptoms and on the basis of each clinical criteria (22–24), 21 were diagnosed with PD, three with MSA, and five with PSP. The remaining six patients had no parkinsonian symptoms: three were clinically diagnosed with Alzheimer's disease (AD), two with spinocerebellar degeneration (SCD), and one with amyotrophic lateral sclerosis (ALS). Table 1 shows the demographic data. The patients with MSA and PSP were classified in the patients with non-PD (NPD) group, while the patients with AD, SCD and ALS were classified in the patients with non-parkinsonian syndromes (NPS) group. The CSF examinations and the ^{11}C-CFT PET scans were performed within 5 months of each other. None of the patients had any concomitant hereditary disorder that could cause parkinsonian symptoms. All the patients were drug naive.

The normal range of HVA was determined by examining the CSF of 13 normal control subjects [five men and eight women; age, 65–88 years (mean = 77.2 years, SD = 8.2)]. Similarly, the normal range for nigrostriatal dopaminergic function was determined by performing ^{11}C-CFT PET scans of eight normal control subjects [five men and three women; age, 55–74 years (mean age = 62.3 years, SD = 6.9)]. All the control subjects were healthy and did not have any underlying diseases or abnormities, as determined on the basis of their medical history and their physical and neurological examinations. None of them were on any medications at the time of the study. All the subjects also underwent routine MRI examinations.

All the CSF examinations and ^{11}C-CFT PET scans were performed for research. This study protocol was approved by the Ethics Committee of the Tokyo Metropolitan Institute of Gerontology and written informed consents were obtained from all the participants.

CSF analysis

Lumbar puncture was performed in the lateral decubitus position to obtain CSF samples from each subject. The first few milliliter of CFS was discarded. The next 3 ml of CFS was used for routine determinations of cell counts, protein and sugar and an additional 2 ml was stored at −70°C until the assays were preformed. The concentration of CSF HVA was measured by injecting 80 μl CSF

Table 1 Demographics of patients and control subjects

	Subjects					
	n	M:F	Age (years)	Duration (years)	Striatal uptake of ^{11}C-CFT (Uptake ratio index)	CSF HVA (ng/ml)
Parkinson's disease	21	11:10	72.9 ± 5.0	1.8 ± 1.3	0.94 ± 0.20	12.8 ± 9.35
Hoehn-Yahr 1	1	1:0	62	1	1.38	36.8
Hoehn-Yahr 2	8	4:4	71.6 ± 4.6	1.4 ± 0.9	1.03 ± 0.14	15.6 ± 9.4
Hoehn-Yahr 3	12	6:6	74.7 ± 3.9	2.1 ± 1.5	0.85 ± 0.17	8.9 ± 5.4
Non-Parkinson's disease	8	4:4	70.5 ± 7.7	1.6 ± 0.8	1.00 ± 0.19	16.4 ± 7.7
Non-parkinsonian syndromes	6	4:2	68.8 ± 6.3	4.5 ± 2.4	2.48 ± 0.28	31.9 ± 13.0
Control for PET study	8	5:3	62.3 ± 6.9		2.68 ± 0.44	
Control for CSF study	13	5:8	77.2 ± 8.2			36.0 ± 13.8

Data are expressed as mean ± SD; *n* = number, CSF, cerebrospinal fluid; HVA, homovanillic acid.

samples into a high-performance liquid chromatography system equipped with 16 electrochemical sensors (CEAS Model 5500; ESA, Bedford, MA, USA), as described previously (14).

PET imaging

^{11}C-CFT PET data acquisition – PET studies were performed at the Positron Medical Center, Tokyo Metropolitan Institute of Gerontology using a SET 2400W scanner (Shimadzu, Kyoto, Japan) in the three-dimensional scanning mode (25). The ^{11}C-CFT was prepared as described previously (26). Each subject received an intravenous bolus injection of 388 ± 75 (mean ± SD) MBq of ^{11}C-CFT. Each subject was then placed in the supine position with their eyes closed in the PET camera gantry. The head was immobilized with a customized head holder in order to align the orbitomeatal line parallel to the scanning plane. To measure the uptake of ^{11}C-CFT, a static scan was performed for 75–90 min after the injection. The specific activity at the time of injection ranged from 7.1–119.6 GBq/μmol. The transmission data were acquired using a rotating ^{68}Ga/^{68}Ge rod source for attenuation correction. Images of 50 slices were obtained with a resolution of 2 × 2 × 3.125 mm voxels and a 128 × 128 matrix.

Analysis of ^{11}C-CFT PET images – Image manipulations were carried out by using the Dr View software (version R2.0; AJS, Tokyo, Japan). The individual PET images were resliced in the transaxial direction, parallel to the anterior–posterior intercommissural (AC–PC) line. Circular regions of interest (ROIs) were placed with reference to the brain atlas and individual MRI images. Five ROIs (diameter, 8 mm) were placed on the striatum on both the left and right sides in each of the three contiguous slices (the AC–PC plane, and regions 3.1 and 6.2 mm above the AC–PC line). Of the five ROIs, one ROI was placed on the caudate and four on the putamen. A total of 50 ROIs (diameter, 10 mm) were selected throughout the cerebellar cortex in five contiguous slices. To evaluate the striatal uptake of ^{11}C-CFT, we calculated the uptake ratio index by the following formula (17, 18), as previously validated (27, 28).

$$\text{Uptake ratio index} = (\text{activity in the striatum} - \text{activity in the cerebellum}) / (\text{activity in the cerebellum}).$$

Statistical analysis

Differences in the averages were tested using a Student's *t*-test. Correlations between the two groups were assessed by linear regression analysis with Pearson's correlation test. $P < 0.01$ was considered to indicate statistical significance.

Results

The inter-individual variability in the concentrations of CSF HVA in each group was relatively large (Fig. 1A). CSF HVA concentrations in both the PD ($P < 0.01$) and NPD groups ($P < 0.01$) were significantly lower than that in the control group (mean ± 2SD, 36.0 ± 27.6), while no significant difference was observed between the NPS and control groups.

The striatal uptake of ^{11}C-CFT in the PD and NPD groups was below the normal range (mean ± 2SD, 2.68 ± 0.87; Fig. 1B). In the PD group, CSF HVA concentrations were significantly

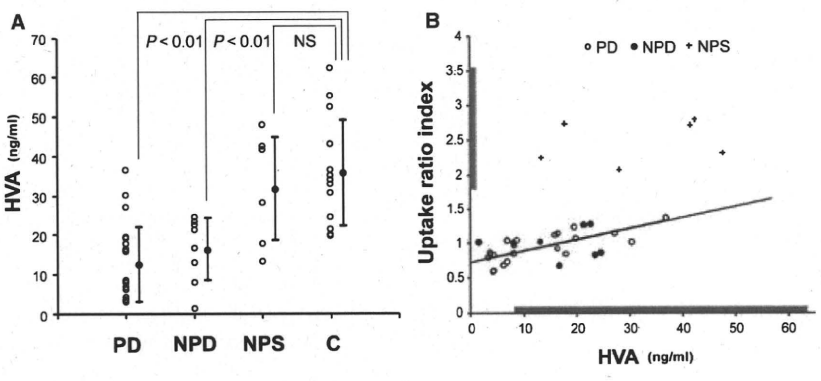

Figure 1. (A) The comparison of CSF HVA concentrations among the disease and control groups. Vertical bars represent mean ± SD. (B) Relationship between CSF HVA concentrations and the striatal uptake of ^{11}C-CFT. A solid line represents the regression line for the PD group. Linear correlation was significant ($r = 0.76$; $P < 0.01$). The grey bars beside the *x*- and *y*-axes represent the normal range (mean ± 2SD) for HVA (36.0 ± 27.6) and the striatal uptake of ^{11}C-CFT (2.68 ± 0.87). PD, Parkinson's disease; NPD, non-Parkinson's disease with parkinsonism; NPS, non-parkinsonian syndromes; C, controls; NS, not significant; CSF, cerebrospinal fluid; HVA, homovanillic acid.

correlated with the striatal uptake of ^{11}C-CFT ($r = 0.76$, $P < 0.01$). In the NPD group, although the correlation between the two indices was not statistically significant, the distribution pattern between the two indexes showed the same tendency as that in the PD group. However, in the NPS group, both CSF HVA concentrations and the striatal uptake of ^{11}C-CFT were within the normal ranges.

Discussion

We evaluated the correlation between CSF HVA concentrations and nigrostriatal dopaminergic function by performing ^{11}C-CFT PET scans. ^{11}C-CFT PET scans showed that all patients with PD and NPD had the dysfunction of nigrostriatal dopaminergic system and all patients with NPS had normal function. The CSF HVA concentrations of all patients with PD and NPD were significantly lower than those of normal subjects, in accordance with previous studies (5–12, 14, 15), whereas, there was no significant difference in CSF HVA concentrations between normal subjects and patients with NPS. These results suggest that CSF HVA concentrations could reflect nigrostriatal dopaminergic function. However, in accordance with previous reports (1–9, 13, 14), all groups showed large inter-individual variability in CSF HVA concentrations and relatively wide overlaps among groups were found. Therefore, in clinical practice, measuring CSF HVA concentrations may be of limited value in the diagnosis of PD.

This is the first study that investigated the correlation between CSF HVA concentrations and nigrostriatal dopaminergic dysfunction. Regardless of relatively high inter-individual variability, CSF HVA concentrations in the PD group showed a considerably high correlation with the striatal uptake of ^{11}C-CFT. The NPD group with nigrostriatal dopaminergic dysfunction showed the same tendency as the PD group, although without significant correlation probably because of the small number of patients. On the other hand, the NPD group with normal nigrostriatal dopaminergic function showed normal ranges in both the HVA level and the striatal uptake of ^{11}C-CFT. Therefore, CSF HVA concentrations may be an additional surrogate maker for estimating the nigrostriatal dopaminergic function in patients with PD, in case that DAT imaging, which has been recognized as a standard maker for the diagnosis of PD, is unavailable.

It is important to note that the DAT images of patients with PD are unique; in the pre-symptomatic phase the reduction in the availability of striatal DAT was detected, presumably as a result of both the degeneration of nigral dopaminergic cells and the compensatory downregulation of DATs on the presynaptic site to maintain normal synaptic dopamine concentrations (17–21). Furthermore, the striatal DAT availability declined at an annual rate of 5–10% (19, 21, 29–31).

Considering our results and the unique characteristics of the DAT images, a possible explanation about the association between CSF HVA concentrations and the striatal uptake of ^{11}C-CFT is as follows (Fig. 2). The first stage of the disease is a compensatory and asymptomatic phase. Along with the progression of nigrostriatal degeneration, the striatal DAT availability begins to decrease, as described earlier (17–21). However, due to several compensatory mechanisms, including the downregulation of DATs and the upregulation of dopamine synthesis, the striatal dopamine concentrations are kept within the normal range (32). As a result, CSF HVA concentrations are also kept in the normal range because CSF HVA is the major end-product of striatal dopamine metabolism. This phase would show relatively large intra-individual and inter-individual variability in CSF HVA concentrations, as observed in subjects with normal nigrostriatal dopaminergic function, because of the reserve capacity for adjusting its levels. The second stage of the progression of the disease is an advanced and symptomatic phase. The compensatory mechanisms to maintain normal synaptic

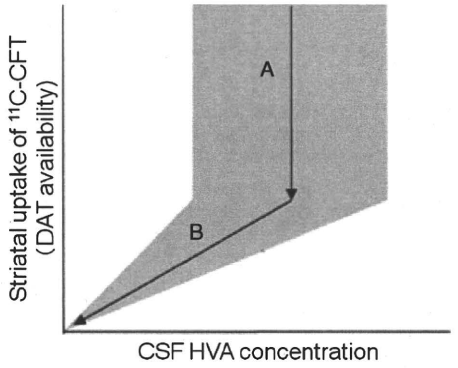

Figure 2. Schematic representation of the mechanism of CSF HVA reduction in patients with PD. (A) The nigrostriatal degeneration begins with a decrease in DAT availability, but due to several compensatory mechanisms, striatal dopamine concentrations (CSF HVA concentrations) are maintained within the normal range. There is a large variability with regard to CSF HVA concentrations. (B) The compensatory mechanisms break down and striatal dopamine concentrations (CSF HVA concentrations) begin to decrease along with the decrease in DAT availability. The variability in CSF HVA concentrations gradually becomes smaller. The grey zone represents the range of variability in CSF HVA concentrations to the striatal uptake of ^{11}C-CFT. DAT, dopamine transporter; CSF, cerebrospinal fluid, HVA, homovanillic acid.